Fuzzy Adaptive Output-Feedback Constrained Trajectory Tracking Control for HFVs with Fixed-Time Convergence

Zuo, Renwei; Li, Yinghui; Lv, Maolong; Liu, Zongcheng; Zhang, Fan

DOI
10.1109/TFUZZ.2022.3161732

Publication date
2022

Document Version
Final published version

Published in
IEEE Transactions on Fuzzy Systems

Fuzzy Adaptive Output-Feedback Constrained Trajectory Tracking Control for HFVs With Fixed-Time Convergence

Renwei Zuo, Yinghui Li, Maolong Lv, Zongcheng Liu, and Fan Zhang

***Abstract*—This article proposes an output-feedback fixed-time trajectory tracking control methodology for hypersonic flight vehicles subject to asymmetric output constraints. In contrast to the state of the art, the most distinguishing feature of our control design lies in avoiding using conventional recursive design methods (e.g., backstepping technique, dynamic surface control, etc.) and in not relying on full-state availability. In the velocity control loop, an asymmetric integral barrier Lyapunov function is adopted to confine velocity variable within a well-defined compact set all the time. In the altitude control loop, after utilizing its cascaded property and proposing a novel scaling function, the original constrained system is transformed to an unconstrained one, which facilitates the control design and stability analysis. Moreover, the proposed control algorithm only involves one fuzzy logic approximator as well as one fixed-time differentiator in the transformed system and guarantees that the tracking errors of velocity and altitude converge into the user-defined residual sets within fixed time. Several comparative simulations have been conducted to highlight the superiorities of the developed method.**

***Index Terms*—Asymmetric output constraints, fixed-time differentiator, hypersonic flight vehicles (HFVs), output-feedback control.**

I. Introduction

HYPERSONIC flight vehicles (HFVs) possess the aerodynamic configuration of high lift-to-drag ratio, which can be launched into the suborbital trajectory either by a booster rocket or by a reusable launch vehicle [1]–[5]. Owing to the rapid response as well as flexible maneuverability, HFVs are recognized as a viable tool in terms of long-range strike, prompt penetration, remote delivery, and power projection [6]. Stemming from the salient characteristics of tightly integrated airframe engine design, hypersonic flight speed, and time-varying flight condition, the dynamical behaviors of HFVs have some special features in comparison with traditional aeronautic aircraft, such as stronger couplings and bigger uncertainties, which bring unprecedented difficulties and challenges to flight control design [7].

In view of the physical constraints that characterize hypersonic flight and operability of scramjet engines, the flight state variables, including velocity and altitude, have upper and lower magnitude constraints in practice, and the violation of these constraints may deteriorate system performance and even endanger flight safety. In the presence of state constraints, a barrier Lyapunov function (BLF) first [8]–[10] and an integral barrier Lyapunov function (IBLF) later [11], [12] are exploited to guarantee the nonviolation of state constraints, while ensuring closed-loop stability. Despite the successful handling of state constraints in [8]–[12], these works followed a standard backstepping design procedure, which inevitably suffers from "explosion of complexity" issue caused by a repeated differentiation of intermediate control laws. Dynamic surface control (DSC) is developed in [13] to tackle such drawback through introducing a low-order filter at each step. However, the methodology in [13] still follows a recursive pattern, exhibiting a complicated design procedure and causing heavy computation burden [14]. Based on the availability of full-state information, backstepping-free control approaches have been proposed in [14]–[17] by transforming the original system into a normal form with full relative degree with respect to system output and its derivatives.

However, it is worth underlining that the precise attitude angle information is typically difficult to be acquired in actual hypersonic flight due to the complicated plant characteristics and drastic variation of flight condition [18]. In the absence of full-state information, output-feedback control algorithms have been constructed [18]–[21] without convergence time guarantees. In view of high speed and agile maneuvering of HFVs, fast convergence is necessarily required for hypersonic flight control. The convergence rate can be preassigned beforehand via the so-called finite [22]–[25] or fixed-time tracking concepts [26]–[29]. It is well recognized that fixed-time stability is a stronger result than finite-time stability since its convergence time is upper bounded by a positive constant irrespective of initial conditions. Even though some fixed-time results have appeared in the literature [26]–[29], the control design there

Manuscript received 8 September 2021; revised 24 December 2021; accepted 17 March 2022. Date of publication 23 March 2022; date of current version 1 November 2022. This work was supported in part by the Excellent Doctoral Dissertation Foundation of Air Force Engineering University under Grant KGD081120005 and in part by the Young Talent Promotion Program of Xi'an under Grant 095920201309. *(Corresponding authors: Yinghui Li; Maolong Lv.)*

Renwei Zuo, Yinghui Li, and Zongcheng Liu are with the Aviation Engineering School, Air Force Engineering University, Xi'an 710038, China (e-mail: zuorenwei0216@163.com; liyinghui66@163.com; liu434853780@163.com).

Maolong Lv is with the Air Traffic Control and Navigation School, Air Force Engineering University, Xi'an 710051, China (e-mail: m.lyu@tudelft.nl).

Fan Zhang is with the Aeronautics and Astronautics School, Sun Yat-sen University, Guangzhou 510275, China (e-mail: zhangfan6@mail.sysu.edu.cn).

Color versions of one or more figures in this article are available at https://doi.org/10.1109/TFUZZ.2022.3161732.

Digital Object Identifier 10.1109/TFUZZ.2022.3161732

is under a recursive manner, and no state constraints are taken into account either.

Motivated by above discussions, a nonrecursive adaptive output-feedback fixed-time trajectory tracking control methodology is proposed in this study.

1) The remarkable peculiarity is that the recursive design procedure (e.g., backstepping technique, DSC, etc.) is circumvented, and the full-state information of HFVs is no longer required for flight control design.
2) To simultaneously handle asymmetric output constraints and "explosion of complexity" issue, we convert the original constrained system to an unconstrained one by resorting to the cascaded feature of altitude dynamics and a novel scaling function.
3) Without devising any virtual control law or command filter, only one fuzzy logic approximator and one fixed-time differentiator are involved to ensure the fixed-time trajectory tracking, which significantly reduces the burden of online computation.

Notations: Throughout this article, $\mathbb{R}$ stands for the set of real numbers, $\mathbb{N}^+$ represents the set of positive integers, $i \in \mathbb{N}_{0:n}$ denotes $i = 0, 1, \ldots, n$, $||\cdot||$ represents the Euclidean norm for vectors, $|\cdot|$ means the absolute value for scalars, $\boldsymbol{I}_n$ is the identity matrix in the space $\mathbb{R}^{n\times n}$, $\boldsymbol{0}_n$ stands for a vector of zeros of dimension n, $[\![\cdot]\!]^l$ implies $|\cdot|^l \mathrm{sgn}(\cdot)$, $(f \circ g)(x)$ represents the composite function, i.e., $(f \circ g)(x) = f(g(x))$, $\log(x)$ denotes the natural logarithm of x, and $\lambda_{\min}(\boldsymbol{A})$ and $\lambda_{\max}(\boldsymbol{A})$ are the minimum and maximum eigenvalues of the matrix $\boldsymbol{A}$, respectively. For ease of notation, the argument in a variable or function sometimes is dropped if no confusion occurs. For example, we abbreviate $\beta(V)$ by β or $\beta(\cdot)$.

II. Vehicle Model and Problem Formulation

A. HFVs Dynamics

The model studied in this article is developed by Bolender and Doman [6] and Parker *et al.* [30] for the longitudinal dynamics of flexible HFVs. Similarly to [2]–[6], we consider hypersonic cruising regimes and leave out ascent and reentry maneuvers for the vehicle model. Assuming a flat Earth and normalizing by the span of the vehicle to unit depth [7], the longitudinal dynamics can be described by a set of differential equations as follows:

$$\begin{aligned}
\dot{V} &= \frac{T\cos\alpha - D}{m} - g\sin\gamma, \quad \dot{h} = V\sin\gamma \\
\dot{\gamma} &= \frac{L + T\sin\alpha}{mV} - \frac{g\cos\gamma}{V}, \quad \dot{\alpha} = Q - \dot{\gamma} \\
\dot{Q} &= \frac{M}{I_{yy}}, \quad \ddot{\eta}_i = -2\zeta_i\omega_i\dot{\eta}_i - \omega_i^2\eta_i + N_i,\ i \in \mathbb{N}_{1:n}
\end{aligned} \tag{1}$$

where rigid-body states V, h, γ, α, and Q denote velocity, altitude, flight path angle (FPA), angle of attack (AOA), and pitch rate, respectively. Flexible state η_i denotes amplitude of the ith bending mode, which is obtained by modeling the fuselage as a single flexible structure with mass-normalized mode shape. m, I_{yy}, g, ζ_i, and ω_i represent vehicle mass, moment of inertia, gravitational acceleration, damping ratio, and flexible mode frequency, respectively. L, D, T, M, and N_i denote lift, drag, thrust, pitching moment, and generalized elastic force, respectively. The approximations of these forces and moment are given as

$$\begin{aligned}
N_i &\approx \bar{q}S\left[N_i^{\alpha^2}\alpha^2 + N_i^{\alpha}\alpha + N_i^{\delta_e}\delta_e + N_i^{\delta_c}\delta_c + N_i^0 + \boldsymbol{N}_i^{\boldsymbol{\eta}}\boldsymbol{\eta}\right] \\
L &\approx \bar{q}SC_L(\alpha, \delta_e, \delta_c, \boldsymbol{\eta}),\ D \approx \bar{q}SC_D(\alpha, \delta_e, \delta_c, \boldsymbol{\eta}) \\
T &\approx \bar{q}S\left[C_{T,\Phi}(\alpha)\Phi + C_T(\alpha) + \boldsymbol{C}_T^{\boldsymbol{\eta}}\boldsymbol{\eta}\right] \\
M &\approx z_T T + \bar{q}S\bar{c}C_M(\alpha, \delta_e, \delta_c, \boldsymbol{\eta})
\end{aligned} \tag{2}$$

where $\boldsymbol{\eta} = [\eta_1, \dot{\eta}_1, \ldots, \eta_n, \dot{\eta}_n]^\top, n \in \mathbb{N}^+$. $\bar{q}, S, z_T$, and $\bar{c}$ denote dynamic press, reference area, thrust moment arm, and reference length, respectively. Φ, δ_e, and δ_c represent fuel equivalence ratio, deflection of elevator, and deflection of canard, which are the control inputs of the HFV dynamics. The curve-fitted approximation coefficients are expressed as

$$\begin{aligned}
C_M &= C_M^{\alpha^2}\alpha^2 + C_M^{\alpha}\alpha + C_M^{\delta_e}\delta_e + C_M^{\delta_c}\delta_c + C_M^0 + \boldsymbol{C}_M^{\boldsymbol{\eta}}\boldsymbol{\eta} \\
C_L &= C_L^{\alpha}\alpha + C_L^{\delta_e}\delta_e + C_L^{\delta_c}\delta_c + C_L^0 + \boldsymbol{C}_L^{\boldsymbol{\eta}}\boldsymbol{\eta} \\
C_D &= C_D^{\alpha^2}\alpha^2 + C_D^{\alpha}\alpha + C_D^{\delta_e^2}\delta_e^2 + C_D^{\delta_e}\delta_e \\
&\quad + C_D^{\delta_c^2}\delta_c^2 + C_D^{\delta_c}\delta_c + C_D^0 + \boldsymbol{C}_D^{\boldsymbol{\eta}}\boldsymbol{\eta} \\
C_{T,\Phi} &= C_{T,\Phi}^{\alpha^3}\alpha^3 + C_{T,\Phi}^{\alpha^2}\alpha^2 + C_{T,\Phi}^{\alpha}\alpha + C_{T,\Phi}^0 \\
C_T &= C_T^{\alpha^3}\alpha^3 + C_T^{\alpha^2}\alpha^2 + C_T^{\alpha}\alpha + C_T^0 \\
\boldsymbol{C}_j^{\boldsymbol{\eta}} &= \left[C_j^{\eta_1}, 0, \ldots, C_j^{\eta_n}, 0\right],\ j \in \{T, M, L, D\} \\
\boldsymbol{N}_i^{\boldsymbol{\eta}} &= \left[N_i^{\eta_1}, 0, \ldots, N_i^{\eta_n}, 0\right],\ i \in \mathbb{N}_{1:n}.
\end{aligned} \tag{3}$$

Herein, to cancel the lift-elevator coupling, δ_c is set to be ganged with δ_e, i.e., $\delta_c = k_{e,c}\delta_e, k_{e,c} = -C_L^{\delta_e}/C_L^{\delta_c}$ [23]. Thereby, the control inputs of HFVs become Φ and δ_e. As a consequence of the physical limitations and performance specifications, the outputs V and h are bound to remain within the following feasible set:

$$\Omega_0 \triangleq \left\{(V, h) \,\middle|\, V_{\min} < V < V_{\max},\ h_{\min} < h < h_{\max}\right\} \tag{4}$$

where $\star_{\max}$ and $\star_{\min}$ are positive constants representing the upper and lower bounds of V and h, respectively. For flight safety and reliability, the reference trajectories V_r and h_r are confined to a subset $\Omega_r \subset \Omega_0$.

The control objective of this study is to design an output-feedback fixed-time trajectory tracking controller such that: 1) the tracking errors of velocity and altitude converge into the user-defined residual sets within fixed time; 2) all flight state variables of the resulting closed-loop system are semiglobally uniformly ultimately bounded (SGUUB); and 3) the asymmetric output constraints (4) are never violated.

B. Model Decomposition

Taking model uncertainties, external disturbances, and structural flexibility into account, the velocity dynamics is formulated

as [15], [16]

$$\dot{V} = \boldsymbol{\zeta}_V^\top(\boldsymbol{f}_V + \boldsymbol{g}_V\Phi) + d_V \tag{5}$$

where

$$\begin{aligned}
\boldsymbol{\zeta}_V =& \frac{S}{m}\Big[C_{T,\Phi}^{\alpha^3}, C_{T,\Phi}^{\alpha^2}, C_{T,\Phi}^{\alpha}, C_{T,\Phi}^{0}, C_{T}^{\alpha^3}, C_{T}^{\alpha^2}, C_{T}^{\alpha}, C_{T}^{0}, C_{D}^{\alpha^2},\\
& C_D^{\alpha}, \left(C_D^{\delta_e^2} + k_{e,c}^2 C_D^{\delta_c^2}\right), \left(C_D^{\delta_e} + k_{e,c} C_D^{\delta_c}\right), C_D^0, \frac{m}{S}\Big]^\top\\
\boldsymbol{f}_V =& \bar{q}\left[\mathbf{0}^{1\times 4}, \alpha^3\cos\alpha, \alpha^2\cos\alpha, \alpha\cos\alpha, \cos\alpha,\right.\\
& \left.-\alpha^2, -\alpha, -\delta_e^2, -\delta_e, -1, -g\sin\gamma/\bar{q}\right]^\top\\
\boldsymbol{g}_V =& \bar{q}\cos\alpha\left[\alpha^3, \alpha^2, \alpha, 1, \mathbf{0}^{1\times 10}\right]^\top
\end{aligned}$$

and the lumped disturbances d_V, brought by model uncertainties, external disturbances such as gust, turbulence, and atmospheric disturbances, as well as structural flexibility from the aerothermoelastic effects, can be expressed as $d_V = \Delta_V + \frac{\bar{q}S}{m}\boldsymbol{C}_T^{\boldsymbol{\eta}}\boldsymbol{\eta}\cos\alpha - \frac{\bar{q}S}{m}\boldsymbol{C}_D^{\boldsymbol{\eta}}\boldsymbol{\eta}$, with Δ_V denoting the model uncertainties and external disturbances in velocity dynamics.

From the viewpoint of engineering, FPA γ is quite small during the cruise phase; thus, we take $\sin\gamma \approx \gamma$ for simplicity [29]. In addition, AOA α is sufficiently small such that the term $T\sin\alpha$ is far smaller than the lift L; thus, $T\sin\alpha$ can be neglected in (1) [9]. As such, the altitude dynamics can be transformed into [15], [16]

$$\begin{cases}
\dot{h} = V\gamma + d_h\\
\dot{\gamma} = \boldsymbol{\zeta}_\gamma^\top(\boldsymbol{f}_\gamma + \boldsymbol{g}_\gamma\alpha) + d_\gamma\\
\dot{\alpha} = \boldsymbol{\zeta}_\alpha^\top(\boldsymbol{f}_\alpha + \boldsymbol{g}_\alpha Q) + d_\alpha\\
\dot{Q} = \boldsymbol{\zeta}_Q^\top(\boldsymbol{f}_Q + \boldsymbol{g}_Q\delta_e) + d_Q
\end{cases} \tag{6}$$

where

$$\begin{aligned}
\boldsymbol{\zeta}_\gamma =& \left[\frac{S}{m}C_L^\alpha, \frac{S}{m}C_L^0, 1\right]^\top,\ \boldsymbol{\zeta}_\alpha = \left[1, \frac{S}{m}C_L^\alpha, \frac{S}{m}C_L^0, 1\right]^\top\\
\boldsymbol{\zeta}_Q =& \frac{S}{I_{yy}}\Big[\bar{c}C_M^{\delta_e}, \bar{c}k_{e,c}C_M^{\delta_c}, z_T C_{T,\Phi}^{\alpha^3}, z_T C_{T,\Phi}^{\alpha^2}, z_T C_{T,\Phi}^{\alpha}, z_T C_{T,\Phi}^{0}\\
& z_T C_T^{\alpha^3}, \left(z_T C_T^{\alpha^2} + \bar{c}C_M^{\alpha^2}\right), \left(z_T C_T^{\alpha} + \bar{c}C_M^{\alpha}\right), \left(z_T C_T^{0} + \bar{c}C_M^{0}\right)\Big]^\top\\
\boldsymbol{g}_\gamma =& \left[\frac{\bar{q}}{V}, \mathbf{0}^{1\times 2}\right]^\top,\ \boldsymbol{g}_\alpha = \left[1, \mathbf{0}^{1\times 3}\right]^\top,\ \boldsymbol{g}_Q = \left[\bar{q}, \bar{q}, \mathbf{0}^{1\times 8}\right]^\top\\
\boldsymbol{f}_\gamma =& \left[0, \frac{\bar{q}}{V}, -\frac{g}{V}\cos\gamma\right]^\top,\ \boldsymbol{f}_\alpha = \frac{\bar{q}}{V}\left[0, -\alpha, -1, \frac{g}{\bar{q}}\cos\gamma\right]^\top\\
\boldsymbol{f}_Q =& \bar{q}\left[\mathbf{0}^{1\times 2}, \alpha^3\Phi, \alpha^2\Phi, \alpha\Phi, \Phi, \alpha^3, \alpha^2, \alpha, 1\right]^\top
\end{aligned}$$

and the lumped disturbances $d_h = \Delta_h$, $d_\gamma = \Delta_\gamma + \frac{\bar{q}S}{mV}\boldsymbol{C}_L^{\boldsymbol{\eta}}\boldsymbol{\eta}$, $d_\alpha = \Delta_\alpha - \frac{\bar{q}S}{mV}\boldsymbol{C}_L^{\boldsymbol{\eta}}\boldsymbol{\eta}$, and $d_Q = \Delta_Q + \frac{z_T\bar{q}S}{I_{yy}}\boldsymbol{C}_T^{\boldsymbol{\eta}}\boldsymbol{\eta} + \frac{\bar{q}S\bar{c}}{I_{yy}} \times \boldsymbol{C}_M^{\boldsymbol{\eta}}\boldsymbol{\eta}$, with Δ_h, Δ_γ, Δ_α, and Δ_Q representing the model uncertainties and external disturbances in altitude dynamics.

C. Technical Key Lemmas

The following results, which are often adopted in control of nonlinear systems, will be used for control design and stability analysis in the subsequent sections.

Lemma 1 (see [26]): Consider a generic dynamical system $\dot{x}(t) = f(t,x)$, $f(t,0) = 0$, $x(0) = x_0$, where $x \in \Omega_x \subset \mathbb{R}^n$, $f: \mathbb{R}^+ \times \Omega_x \to \mathbb{R}^n$, and suppose that the origin is an equilibrium point. If $\Omega_x = \mathbb{R}^n$ and there exists a Lyapunov function $L(x)$ defined on $\mathbb{R}^n$ satisfying

$$\dot{L}(x) \le -\left(\alpha L^p(x) + \beta L^q(x)\right)^\kappa \tag{7}$$

where α, β, p, q, and κ are some positive constants, $p\kappa > 1$, and $q\kappa < 1$, then the origin of the system is fixed-time stable, and the settling time satisfies $T(x_0) \le \frac{1}{\alpha^\kappa(p\kappa-1)} + \frac{1}{\beta^\kappa(1-q\kappa)}$ for a given initial condition $x_0 \in \mathbb{R}^n$.

Especially, if $\kappa = 1$ and there exists a Lyapunov function $L(x)$ defined on $\Omega_{x,0} \subseteq \Omega_x \subset \mathbb{R}^n$ satisfying

$$\dot{L}(x) \le -\alpha L^p(x) - \beta L^q(x) \tag{8}$$

where α, β, $p > 1$, and $q < 1$ are some positive constants, then the origin of the system is locally fixed-time stable, and the settling time satisfies $T(x_0) \le \frac{1}{\alpha(p-1)} + \frac{1}{\beta(1-q)}$ for a given initial condition $x_0 \in \Omega_{x,0}$.

Lemma 2 (see [31]): Let $\chi = \vartheta(\upsilon, \lambda) : \Omega_\upsilon \times \Omega_\lambda \to \Omega_\chi$ be a smooth function with $\Omega_\upsilon \subset \mathbb{R}^n$, $\Omega_\lambda \subset \mathbb{R}$, and $\Omega_\chi \subset \mathbb{R}$; if $\frac{\partial\vartheta(\upsilon,\lambda)}{\partial\lambda} > 0$ and $\frac{\partial\upsilon}{\partial\lambda} = 0$, $\forall\upsilon \in \Omega_\upsilon$, $\lambda \in \Omega_\lambda$, then there exists a smooth function $\phi(\cdot)$ such that $\lambda = \phi(\upsilon, \chi) : \Omega_\upsilon \times \Omega_\chi \to \Omega_\lambda$.

Lemma 3 (see [32]–[34]): For any given positive constants c_0, c_1, and c_2, the following inequality holds:

$$|\xi|^{c_0}|\zeta|^{c_1} \le \frac{c_0 c_2}{c_1 + c_2}|\xi|^{c_0+c_1} + \frac{c_1}{c_1 + c_2}c_2^{-\frac{c_0}{c_1}}|\zeta|^{c_0+c_1} \tag{9}$$

where ξ and ζ are any real variables.

Lemma 4 (see [35]–[37]): Define a set of fuzzy IF–THEN rules, where the lth IF–THEN rule is written as

$$R^l: \text{If } x_1 \text{ is } F_1^l, \text{ and } \ldots \text{ and } x_n \text{ is } F_n^l, \text{ then } y \text{ is } B^l \tag{10}$$

where $\boldsymbol{x} = [x_1, \ldots, x_n]^\top \in \mathbb{R}^n$, and $y \in \mathbb{R}$ are the input and output of the fuzzy logic systems (FLSs), $F_1^l, \ldots, F_n^l$ and B^l are fuzzy sets in $\mathbb{R}$. Let $F(\boldsymbol{x})$ be a continuous function defined on a compact set $\Omega_{\boldsymbol{x}}$. Then, for a given desired level of accuracy $\varepsilon > 0$, there exists an FLS $\boldsymbol{W}^\top\boldsymbol{\varphi}(\boldsymbol{x})$ such that

$$\sup_{\boldsymbol{x}\in\Omega_{\boldsymbol{x}}}|F(\boldsymbol{x}) - \boldsymbol{W}^\top\boldsymbol{\varphi}(\boldsymbol{x})| \le \varepsilon \tag{11}$$

where $\boldsymbol{\varphi}(\boldsymbol{x}) = [\phi_1(\boldsymbol{x}), \ldots, \phi_p(\boldsymbol{x})]^\top$ is the fuzzy basis function vector, and $\phi_l(\boldsymbol{x}) = \prod_{j=1}^n \mu_{F_j^l}(x_j) \big/ \sum_{l=1}^p (\prod_{j=1}^n \mu_{F_j^l}(x_j))$, with $\mu_{F_j^l}(x_j)$ being a fuzzy membership function of the variable x_j in IF–THEN rule. $\boldsymbol{W} = [w_1, \ldots, w_p]^\top$ is the adaptive fuzzy parameter vector, and w_l is the inference variable corresponding to the lth IF–THEN rule. The optimal parameter vector $\boldsymbol{W}^*$ is defined as

$$\boldsymbol{W}^* = \arg\min_{\boldsymbol{W}\in\Omega_{\boldsymbol{W}}}\left\{\sup_{\boldsymbol{x}\in\Omega_{\boldsymbol{x}}}|F(\boldsymbol{x}) - \boldsymbol{W}^\top\boldsymbol{\varphi}(\boldsymbol{x})|\right\} \tag{12}$$

where $\Omega_{\boldsymbol{W}}$ is a compact set for $\boldsymbol{W}$.

III. Velocity Control Loop

This section is aimed at designing a fixed-time output-feedback control scheme for velocity dynamics. We first present the design with a novel asymmetric IBLF.

A. Asymmetric IBLF for Velocity Dynamics

Utilizing the error coordinate $\widetilde{V} = V - V_r$, a new asymmetric IBLF is devised as

$$L_{\widetilde{V}} = \int_0^{\widetilde{V}} \frac{(V_{\max} - V_{\min})^2 \tau}{(V_{\max} - \tau - V_r)(\tau + V_r - V_{\min})} \mathrm{d}\tau \tag{13}$$

where $V_{\max}$ and $V_{\min}$ are positive constants representing the upper and lower bounds of V given in (4). In view of (13), it can be immediately obtained that $\lim_{V \to V_{\max}} L_{\widetilde{V}} = +\infty$, $\lim_{V \to V_{\min}} L_{\widetilde{V}} = +\infty$, $L_{\widetilde{V}} \geq \frac{1}{2}\widetilde{V}^2$, and $L_{\widetilde{V}}$ is continuously differentiable and directly related to state variable. The following lemma is substantial in ensuring constraints satisfaction.

Lemma 5: The asymmetric IBLF $L_{\widetilde{V}}$ in (13) satisfies

$$L_{\widetilde{V}} \leq \frac{(V_{\max} - V_{\min})^2 \widetilde{V}^2}{(V_{\max} - V)(V - V_{\min})} \tag{14}$$

for $V \in \Omega_0$.

Proof: Initially, let us denote

$$U(\tau, V_r) = \frac{(V_{\max} - V_{\min})^2 \tau}{(V_{\max} - \tau - V_r)(\tau + V_r - V_{\min})}.$$

Subsequently, we can show that

$$\frac{\partial U}{\partial \tau} = \frac{(V_{\max} - V_{\min})^2 \left[(V_{\max} - V_r)(V_r - V_{\min}) + \tau^2\right]}{(V_{\max} - \tau - V_r)^2 (\tau + V_r - V_{\min})^2}$$

which is positive definite for $\tau + V_r \in \Omega_0$. Since $U(0, V_r) = 0$ for $V_r \in \Omega_0$, and $U(\tau, V_r)$ is monotonically increasing with respect to τ, the following inequality holds for $V \in \Omega_0$:

$$\int_0^{\widetilde{V}} U(\tau, V_r) \mathrm{d}\tau \leq U(\widetilde{V}, V_r)\widetilde{V}$$

which leads to (14) after substituting for $U(\tau, V_r)$. ■

Then, the time derivative of $L_{\widetilde{V}}$ is

$$\dot{L}_{\widetilde{V}} = \frac{\partial L_{\widetilde{V}}}{\partial \widetilde{V}} \dot{\widetilde{V}} + \frac{\partial L_{\widetilde{V}}}{\partial V_r} \dot{V}_r \tag{15}$$

where $\partial L_{\widetilde{V}}/\partial \widetilde{V} = \beta(V)\widetilde{V}$, $\partial L_{\widetilde{V}}/\partial V_r = \beta(V)\widetilde{V} - \widetilde{V}\xi(\widetilde{V}, V_r)$, with $\xi(\widetilde{V}, V_r) = \int_0^1 \frac{(V_{\max} - V_{\min})^2}{(V_{\max} - \sigma\widetilde{V} - V_r)(\sigma\widetilde{V} + V_r - V_{\min})} \mathrm{d}\sigma$ and $\beta(V) = \frac{(V_{\max} - V_{\min})^2}{(V_{\max} - V)(V - V_{\min})}$.

Incorporating (5) into (15), we arrive at

$$\dot{L}_{\widetilde{V}} = \beta\widetilde{V}\boldsymbol{\zeta}_V^\top (\boldsymbol{f}_V + \boldsymbol{g}_V \Phi) + \widetilde{V} F_V(\boldsymbol{x}_V) - \frac{\widetilde{V}^2}{2} \tag{16}$$

where $F_V(\boldsymbol{x}_V) = \beta d_V - \xi(\widetilde{V}, V_r)\dot{V}_r + \frac{\widetilde{V}}{2}$, and $\boldsymbol{x}_V = [V, V_r, \dot{V}_r]^\top$.

B. Controller Design for Velocity Dynamics

Hereafter, we shall conduct the controller design based on the error dynamics (16). According to Lemma 4, $F_V(\boldsymbol{x}_V)$ can be approximated by an FLS as $F_V(\boldsymbol{x}_V) = \boldsymbol{W}_V^{*\top} \boldsymbol{\varphi}_V(\boldsymbol{x}_V) + \varepsilon_V$, where ε_V is the minimum fuzzy approximation error, and there exists $\varepsilon_V^* \in \mathbb{R}^+$ such that $|\varepsilon_V| \leq \varepsilon_V^*$. The controller for velocity dynamics is devised as

$$\Phi = \frac{1}{\boldsymbol{\zeta}_V^\top \boldsymbol{g}_V} \Bigg(- k_{V,1} \beta^{\frac{p-1}{2}} \widetilde{V}^p - k_{V,2} \beta^{\frac{q-1}{2}} \widetilde{V}^q - \boldsymbol{\zeta}_V^\top \boldsymbol{f}_V - \frac{\widetilde{V}\widehat{\phi}_V}{2a_V^2 \beta} \boldsymbol{\varphi}_V^\top(\boldsymbol{x}_V)\boldsymbol{\varphi}_V(\boldsymbol{x}_V) \Bigg) \tag{17}$$

where $k_{V,1}$ and $k_{V,2}$ are positive design parameters, $\widehat{\phi}_V$ is the estimate of $\phi_V = ||\boldsymbol{W}_V^*||^2$ with estimation error $\widetilde{\phi}_V = \phi_V - \widehat{\phi}_V$, $1 < p = p_1/p_2$, and $0 < q = q_1/q_2 < 1$, with p_1, p_2, q_1, and q_2 being positive odd integers.

The adaptation law is designed as

$$\dot{\widehat{\phi}}_V = -\rho_V \upsilon_V \widehat{\phi}_V + \frac{\rho_V \widetilde{V}^2}{2a_V^2} \boldsymbol{\varphi}_V^\top(\boldsymbol{x}_V)\boldsymbol{\varphi}_V(\boldsymbol{x}_V) \tag{18}$$

where $\rho_V = \frac{2c_V}{2c_V - 1}$, with $c_V > \frac{1}{2}$ a constant, and υ_V is a positive design parameter. The initial value of $\widehat{\phi}_V$ is set as $\widehat{\phi}_V(0) \geq 0$.

To proceed with the stability analysis for velocity dynamics, let us consider the following total Lyapunov function:

$$L_V = L_{\widetilde{V}} + L_{\widetilde{\phi}_V} \tag{19}$$

where $L_{\widetilde{V}}$ is given in (13) and $L_{\widetilde{\phi}_V} = \frac{1}{2\rho_V}\widetilde{\phi}_V^2$. Subsequently, the main results are given as follows.

Theorem 1: Consider the velocity dynamics (5) in the presence of asymmetric output constraints (4). Under the output-feedback control law (17) and adaptation law (18) for any initial condition $V(0) \in \Omega_0$, if $L_V(0) \leq \varrho_V$ holds for any positive constant ϱ_V, then there exist design parameters $k_{V,1}$, υ_V, a_V, and c_V such that: 1) V is driven to track the reference trajectory V_r in fixed time; 2) all the signals in velocity dynamics (5) are SGUUB; and 3) the output constraints (4) are never violated.

Proof: See the Appendix for the proof, which is based on constructing a total Lyapunov function (19) whose time derivative has the same structure as Lemma 1 (43). This guarantees fixed-time convergence for the states in velocity dynamics. ■

Remark 1: In the literature, the following log-type asymmetric BLF is commonly used [8]–[10]:

$$L_{\widetilde{V}} = \frac{1}{2} l(\widetilde{V}) \log \frac{k_1^2}{k_1^2 - \widetilde{V}^2} + \frac{1}{2}\left(1 - l(\widetilde{V})\right) \log \frac{k_2^2}{k_2^2 - \widetilde{V}^2}$$

where $k_1 = V_{\max} - V_{r,\max}$, $k_2 = V_{r,\min} - V_{\min}$, with $V_{r,\max}$ and $V_{r,\min}$ denoting the upper and lower bounds of V_r, respectively, and switching function

$$l(\widetilde{V}) = \begin{cases} 1, & \text{if } \widetilde{V} > 0 \\ 0, & \text{otherwise.} \end{cases}$$

Note that the above common BLF is only dependent on the transformed error bounds k_1 and k_2 rather than the original output bounds $V_{\max}$ and $V_{\min}$, introducing some degree of conservatism. On the contrary, here, we devise a new asymmetric IBLF (13), which utilizes the original output bounds $V_{\max}$ and

$V_{\min}$ directly to guarantee the nonviolation of output constraint $V \in \Omega_0$, achieving significant simplification and relaxation of the control design to some extent.

IV. Altitude Control Loop

From the fact that there exist four rigid-body states (i.e., h, γ, α, and Q) in altitude dynamics (6), the conventional recursive design methods (e.g., backstepping [8], [18], [23], [29]) generally require four iterative steps as well as four control laws and their derivatives, increasing the complexity and computation burden. To handle this issue, a new system transformation is developed to transform the original constrained system (6) into an unconstrained one, while guaranteeing the nonviolation of the output constraints (4).

A. Model Transformation for Altitude Dynamics

Initially, let us devise the following new scaling function:

$$S(h) = \frac{2h - h_{\max} - h_{\min}}{(h - h_{\min})(h_{\max} - h)} \tag{20}$$

where $h_{\max}$ and $h_{\min}$ are positive constants representing the upper and lower bounds of h given in (4), respectively.

Remark 2: To guarantee that the output constraints (4) hold, a new scaling function (20) is constructed, which exhibits the following two distinguishing features: 1) it provides an explicit (direct) way to deal with the output constraints (4), without introducing the transformed error constraints [8]–[10]; and 2) it avoids the use of the piecewise asymmetric BLF as in [8].

Lemma 6: Consider the scaling function $S(h)$ in (20); the following properties hold: 1) for $h \in \Omega_0$, $\frac{\partial S(h)}{\partial h} > 0$, $\lim_{h\to h_{\max}} S(h) = +\infty$, and $\lim_{h\to h_{\min}} S(h) = -\infty$; 2) for $h \in \Omega_0$, $S(h)$ is continuously differentiable with respect to time; and 3) for any initial condition $h(0) \in \Omega_0$, if $S(h) \in L_\infty$, then $h \in \Omega_0$ holds for all $t \in [0, +\infty)$.

Proof: In view of (20), the results $\lim_{h\to h_{\max}} S(h) = +\infty$ and $\lim_{h\to h_{\min}} S(h) = -\infty$ can be immediately obtained, and it is possible to obtain that

$$\psi(h) = \frac{\partial S(h)}{\partial h} = \frac{1}{(h_{\max} - h)^2} + \frac{1}{(h - h_{\min})^2}$$

where $\psi(h)$ is positive definite, i.e., $\frac{\partial S(h)}{\partial h} > 0$ for $h \in \Omega_0$.

Besides, $S^{(i)}(h)$ can be formulated as

$$S^{(i)}(h) = \frac{\Psi_1(h_{\min}, h, \ldots, h^{(i)})}{(h - h_{\min})^{2^i}} + \frac{\Psi_2(h_{\max}, h, \ldots, h^{(i)})}{(h_{\max} - h)^{2^i}}$$

where $\Psi_1(\cdot)$ and $\Psi_2(\cdot)$ are two polynomials and the involved terms therein take the product form of $h_{\max}, h_{\min}, h, \ldots, h^{(i)}$.

Finally, we give the following proof by contradiction. Suppose that $h = h_1$ for $t = t_1$, where $h_1 \le h_{\min}$ or $h_1 \ge h_{\max}$. Since $h(0) \in \Omega_0$ and $h(t)$ is a continuous function, according to the intermediate value theorem [38], there exists a time instant $0 < t_2 < t_1$ such that $h(t_2) \to h_{\max}$ or $h(t_2) \to h_{\min}$. Therefore, $S(h(t_2)) = +\infty$ or $S(h(t_2)) = -\infty$, which leads to a contradiction for the boundedness of $S(h)$. Consequently, $h \in \Omega_0$ holds for all $t \in [0, +\infty)$. ■

Defining a new set of states $\{\chi_i\}$, $i \in \mathbb{N}_{1:4}$, a system transformation is conducted to convert the original constrained altitude dynamics (6) into an unconstrained one. Let $\boldsymbol{\chi}_i = [\chi_1, \ldots, \chi_i]^\top$; then, the details for such transformation are given in the following.

We start with defining an auxiliary state χ_1 in the form of

$$\chi_1 = S(h) \triangleq \ell_1(h). \tag{21}$$

Since $S(h)$ is monotonically increasing with respect to h, it follows from (20) and (21) that

$$h = S^{-1}(\chi_1) \triangleq \varsigma_1(\chi_1) \tag{22}$$

where $\varsigma_1(\cdot)$ is a smooth function with respect to χ_1.

Define an auxiliary state χ_2 in the form of

$$\chi_2 = \dot{\chi}_1 = \frac{\partial \ell_1(h)}{\partial h}\dot{h} = \psi(h)(V\gamma + d_h) \triangleq \ell_2(h, \gamma). \tag{23}$$

Notice by Lemma 6 that $\psi(h)$ is smooth and positive definite for $h \in \Omega_0$; thus, $\ell_2(\cdot)$ is smooth and monotonically increasing with respect to γ. Recalling Lemma 2, there exists a smooth function $\varsigma_2(\cdot)$ such that

$$\gamma \triangleq \varsigma_2(\boldsymbol{\chi}_2). \tag{24}$$

Define an auxiliary state χ_3 in the form of

$$\begin{aligned}\chi_3 = \dot{\chi}_2 &= \frac{\partial \ell_2(h,\gamma)}{\partial h}\dot{h} + \frac{\partial \ell_2(h,\gamma)}{\partial \gamma}\dot{\gamma} \\ &= \vartheta_2(h,\gamma) + \psi(h)V\left(\boldsymbol{\zeta}_\gamma^\top(\boldsymbol{f}_\gamma + \boldsymbol{g}_\gamma\alpha) + d_\gamma\right) \\ &\triangleq \ell_3(h,\gamma,\alpha).\end{aligned} \tag{25}$$

Similarly, applying Lemma 2 to (25) obtains

$$\alpha \triangleq \varsigma_3(\boldsymbol{\chi}_3). \tag{26}$$

At this stage, auxiliary state χ_4 is given by

$$\begin{aligned}\chi_4 = \dot{\chi}_3 &= \frac{\partial \ell_3(\cdot)}{\partial h}\dot{h} + \frac{\partial \ell_3(\cdot)}{\partial \gamma}\dot{\gamma} + \frac{\partial \ell_3(\cdot)}{\partial \alpha}\dot{\alpha} \\ &= \vartheta_3(h,\gamma,\alpha) + \psi(h)V\boldsymbol{\zeta}_\gamma^\top\boldsymbol{g}_\gamma\left(\boldsymbol{\zeta}_\alpha^\top(\boldsymbol{f}_\alpha + \boldsymbol{g}_\alpha Q) + d_\alpha\right) \\ &\triangleq \ell_4(h,\gamma,\alpha,Q).\end{aligned} \tag{27}$$

Similarly and iteratively, applying Lemma 2 to (27) yields

$$Q \triangleq \varsigma_4(\boldsymbol{\chi}_4). \tag{28}$$

Summarizing above analysis, the altitude dynamics (6) can be rewritten into the following compact form:

$$\begin{cases}\dot{\boldsymbol{\chi}}_4 = \boldsymbol{A}\boldsymbol{\chi}_4 + \boldsymbol{B}\left(\vartheta_4(h,\gamma,\alpha,Q) + \psi(h)g_4(h,\gamma,\alpha,Q)\delta_e\right) \\ \chi_1 = \boldsymbol{C}^\top\boldsymbol{\chi}_4\end{cases} \tag{29}$$

where $\boldsymbol{A} = \left[\begin{smallmatrix}\mathbf{0_3} & \boldsymbol{I}_3 \\ 0 & \mathbf{0}_3^\top\end{smallmatrix}\right]$, $\boldsymbol{B} = \left[\begin{smallmatrix}\mathbf{0_3} \\ 1\end{smallmatrix}\right]$, $\boldsymbol{C} = \left[\begin{smallmatrix}1 \\ \mathbf{0}_3\end{smallmatrix}\right]$, $\vartheta_4(\cdot) = \psi(h)V\boldsymbol{\zeta}_\gamma^\top\boldsymbol{g}_\gamma\boldsymbol{\zeta}_\alpha^\top\boldsymbol{g}_\alpha(\boldsymbol{\zeta}_Q^\top\boldsymbol{f}_Q + d_Q) + \frac{\partial \ell_3(\cdot)}{\partial h}\dot{h} + \frac{\partial \ell_3(\cdot)}{\partial \gamma}\dot{\gamma} + \frac{\partial \ell_3(\cdot)}{\partial \alpha}\dot{\alpha}$, and $g_4(\cdot) = V\boldsymbol{\zeta}_\gamma^\top\boldsymbol{g}_\gamma\boldsymbol{\zeta}_\alpha^\top\boldsymbol{g}_\alpha\boldsymbol{\zeta}_Q^\top\boldsymbol{g}_Q$. In view of (22), (24), (26), and (28), (29) can be further represented by

$$\begin{cases}\dot{\boldsymbol{\chi}}_4 = \boldsymbol{A}\boldsymbol{\chi}_4 + \boldsymbol{B}\left(\vartheta_\chi(\boldsymbol{\chi}_4) + \psi_\chi(\chi_1)g_\chi(\boldsymbol{\chi}_4)\delta_e\right) \\ \chi_1 = \boldsymbol{C}^\top\boldsymbol{\chi}_4\end{cases} \tag{30}$$

where $\vartheta_\chi(\boldsymbol{\chi}_4)=(\vartheta_4\circ\varsigma)(\boldsymbol{\chi}_4)$, $g_\chi(\boldsymbol{\chi}_4)=(g_4\circ\varsigma)(\boldsymbol{\chi}_4)$, and $\psi_\chi(\chi_1)=(\psi\circ\varsigma)(\chi_1)$. Since $\psi(\cdot)$ and $g_4(\cdot)$ are positive definite and bounded for $h\in\Omega_0$, one has $\psi_\chi(\chi_1)>0$ and $g_{\chi,\max}\geq g_\chi(\boldsymbol{\chi}_4)\geq g_{\chi,\min}>0$ for $\boldsymbol{\chi}_4\in\Omega_{\boldsymbol{\chi}_4}$, where $g_{\chi,\min}$ and $g_{\chi,\max}$ are positive constants, and $\Omega_{\boldsymbol{\chi}_4}$ is a compact set.

Before moving on, let us first define an auxiliary reference trajectory $h_r^*=S(h_r)$, where $S(\cdot)$ is given in (20). Then, define the corresponding output tracking error $z_h=\chi_1-h_r^*$, and let $\boldsymbol{z}_h=[z_h,z_h^{(1)},z_h^{(2)},z_h^{(3)}]^\top$ and $\boldsymbol{h}_r^*=[h_r^*,h_r^{*(1)},h_r^{*(2)},h_r^{*(3)}]^\top$.

Subsequently, the filtered error s is formulated as

$$s=z_h^{(3)}+\lambda_1 z_h^{(2)}+\lambda_2 z_h^{(1)}+\lambda_3 z_h=[\boldsymbol{\Lambda}\ \ 1]\,\boldsymbol{z}_h \tag{31}$$

where $\boldsymbol{\Lambda}=[\lambda_3,\lambda_2,\lambda_1]$, with λ_1, λ_2, and λ_3 being user-chosen parameters such that the polynomial $q^3+\lambda_1 q^2+\lambda_2 q+\lambda_3$ is Hurwitz. Furthermore, the time derivative of s is

$$\begin{aligned}\dot{s}=&\ [0\ \ \boldsymbol{\Lambda}]\,\boldsymbol{z}_h+\vartheta_\chi(\boldsymbol{\chi}_4)+\psi_\chi(\chi_1)g_\chi(\boldsymbol{\chi}_4)\delta_e-h_r^{*(4)}\\ =&\ \psi_\chi(\chi_1)g_\chi(\boldsymbol{\chi}_4)\delta_e+F_h(\boldsymbol{x}_h)-\frac{1}{2}s\end{aligned} \tag{32}$$

where $F_h(\boldsymbol{x}_h)=[0\ \ \boldsymbol{\Lambda}]\boldsymbol{z}_h+\vartheta_\chi(\boldsymbol{\chi}_4)-h_r^{*(4)}+\frac{1}{2}s$ with $\boldsymbol{x}_h=[\boldsymbol{\chi}_4^\top,\boldsymbol{h}_r^\top]^\top$ and $\boldsymbol{h}_r=[h_r,h_r^{(1)},h_r^{(2)},h_r^{(3)},h_r^{(4)}]^\top$.

Remark 3: In the existing relevant methods [14]–[16], the transformed system nonlinearities are functions with regard to flight states γ, α, and Q, which are difficult to be obtained accurately in practice. To tackle this issue, we introduce some new state variables $\boldsymbol{\chi}_4$, based on which an output-feedback control framework is established later without involving any original flight state variables γ, α, and Q.

B. Controller Design for Altitude Dynamics

Hereafter, we shall conduct the controller design on the basis of the error dynamics (32). Initially, let us introduce a fixed-time differentiator to estimate the unavailable state variables $\boldsymbol{\chi}_4$ as follows:

$$\begin{cases}\dot{\widehat{\chi}}_1=\ \widehat{\chi}_2-\tau_1\left[\![\widehat{\chi}_1-\chi_1]\!\right]^{p_1}-\iota_1\left[\![\widehat{\chi}_1-\chi_1]\!\right]^{q_1}\\ \dot{\widehat{\chi}}_2=\ \widehat{\chi}_3-\tau_2\left[\![\widehat{\chi}_1-\chi_1]\!\right]^{p_2}-\iota_2\left[\![\widehat{\chi}_1-\chi_1]\!\right]^{q_2}\\ \dot{\widehat{\chi}}_3=\ \widehat{\chi}_4-\tau_3\left[\![\widehat{\chi}_1-\chi_1]\!\right]^{p_3}-\iota_3\left[\![\widehat{\chi}_1-\chi_1]\!\right]^{q_3}\\ \dot{\widehat{\chi}}_4=\ -\tau_4\left[\![\widehat{\chi}_1-\chi_1]\!\right]^{p_4}-\iota_4\left[\![\widehat{\chi}_1-\chi_1]\!\right]^{q_4}\end{cases} \tag{33}$$

where the positive design parameters $p_i>1$ and $q_i<1$, $i\in\mathbb{N}_{1:4}$, satisfy the recurrent relations $p_i=ip_1-i+1$ and $q_i=iq_1-i+1$, $i\in\mathbb{N}_{2:4}$, with $p_1\in(1,1+\varepsilon_p)$ and $q_1\in(1-\varepsilon_q,1)$ for the sufficiently small positive constants ε_p and ε_q. Furthermore, the differentiator gains τ_i and ι_i, $i\in\mathbb{N}_{1:4}$, are selected such that the matrices

$$\boldsymbol{\Gamma}_1=\begin{bmatrix}-\tau_1&1&0&0\\-\tau_2&0&1&0\\-\tau_3&0&0&1\\-\tau_4&0&0&0\end{bmatrix},\ \boldsymbol{\Gamma}_2=\begin{bmatrix}-\iota_1&1&0&0\\-\iota_2&0&1&0\\-\iota_3&0&0&1\\-\iota_4&0&0&0\end{bmatrix}$$

are Hurwitz; then, the following lemma holds.

Lemma 7: Consider the differentiator (33), the error vector $\widetilde{\boldsymbol{\chi}}_4=[\widetilde{\chi}_1,\widetilde{\chi}_2,\widetilde{\chi}_3,\widetilde{\chi}_4]^\top$ with $\widetilde{\chi}_i=\chi_i-\widehat{\chi}_i$, $i\in\mathbb{N}_{1:4}$, can converge to the origin in fixed time

$$T_1\leq T_{1,\max}\triangleq\frac{\lambda_{\max}^{2-q_1}(\boldsymbol{P}_2)}{(1-q_1)\lambda_{\min}(\boldsymbol{Q}_2)}+\frac{\lambda_{\max}(\boldsymbol{P}_1)}{(p_1-1)\xi^{p_1-1}\lambda_{\min}(\boldsymbol{Q}_1)}$$

where the positive constant $\xi\leq\lambda_{\min}(\boldsymbol{P}_1)$, and the symmetric positive-definite matrices $\boldsymbol{P}_1$, $\boldsymbol{P}_2$, $\boldsymbol{Q}_1$, and $\boldsymbol{Q}_2$ satisfy

$$\boldsymbol{P}_1\boldsymbol{\Gamma}_1+\boldsymbol{\Gamma}_1\boldsymbol{P}_1=-\boldsymbol{Q}_1,\quad \boldsymbol{P}_2\boldsymbol{\Gamma}_2+\boldsymbol{\Gamma}_2\boldsymbol{P}_2=-\boldsymbol{Q}_2$$

where the matrices $\boldsymbol{\Gamma}_1$ and $\boldsymbol{\Gamma}_2$ are defined after (33).

Proof: The proof of Lemma 7 is similar to [39, Th. 3] and is omitted here for space limitations. ■

From Lemma 4, the unknown system dynamics $F_h(\boldsymbol{x}_h)$ can be approximated by an FLS as $F_h(\boldsymbol{x}_h)=\boldsymbol{W}_h^{*\top}\boldsymbol{\varphi}_h(\boldsymbol{x}_h)+\varepsilon_h$, where ε_h is the minimum fuzzy approximation error, and there exists $\varepsilon_h^*\in\mathbb{R}^+$ such that $|\varepsilon_h|\leq\varepsilon_h^*$. Then, we use state estimates to devise the output-feedback control law δ_e as

$$\delta_e=\frac{1}{\psi_\chi}\left(-k_{h,1}\widehat{s}^p-k_{h,2}\widehat{s}^q-\frac{\widehat{s}\widehat{\phi}_h}{2a_h^2}\boldsymbol{\varphi}_h^\top(\widehat{\boldsymbol{x}}_h)\boldsymbol{\varphi}_h(\widehat{\boldsymbol{x}}_h)\right) \tag{34}$$

where $k_{h,1}$ and $k_{h,2}$ are positive design parameters, $\widehat{\boldsymbol{x}}_h=[\widehat{\boldsymbol{\chi}}_4^\top,\boldsymbol{h}_r^\top]^\top$ with $\widehat{\boldsymbol{\chi}}_4=[\widehat{\chi}_1,\widehat{\chi}_2,\widehat{\chi}_3,\widehat{\chi}_4]^\top$, and $\widehat{\phi}_h$ is the estimate of $\phi_h=||\boldsymbol{W}_h^*||^2$ with estimation error $\widetilde{\phi}_h=\phi_h-g_{\chi,\min}\widehat{\phi}_h$.

The adaptation law is designed as

$$\dot{\widehat{\phi}}_h=-\upsilon_h\rho_h\widehat{\phi}_h+\frac{\rho_h\widehat{s}^2}{2a_h^2}\boldsymbol{\varphi}_h^\top(\widehat{\boldsymbol{x}}_h)\boldsymbol{\varphi}_h(\widehat{\boldsymbol{x}}_h) \tag{35}$$

where $\rho_h=\frac{2c_h}{2c_h-1}$ with $c_h>\frac{1}{2}$ a constant, and υ_h is a positive design parameter. The initial value of $\widehat{\phi}_h$ is set as $\widehat{\phi}_h(0)\geq 0$.

To proceed with the stability analysis for altitude dynamics, let us consider the following total Lyapunov function:

$$L_h=L_s+L_{\widetilde{\phi}_h} \tag{36}$$

where $L_s=\frac{1}{2}s^2$ and $L_{\widetilde{\phi}_h}=\frac{1}{2\rho_h}\widetilde{\phi}_h^2$. Subsequently, the main results are given as follows.

Theorem 2: Consider the altitude dynamics (6) in the presence of asymmetric output constraints (4). Under the differentiator-based output-feedback control law (34) and adaptation law (35) for any initial condition $h(0)\in\Omega_0$, if $L_h(0)\leq\varrho_h$ holds for any positive constant ϱ_h, then there exist design parameters $k_{h,1}$, υ_h, a_h, and c_h such that: 1) the filtered tracking error $s(t)$ converges into an adjustable residual set around zero in fixed time; 2) all the signals in altitude dynamics (6) are SGUUB; and 3) the output constraints (4) are never violated.

Proof: See the Appendix for the proof, which is based on constructing a total Lyapunov function (36) whose time derivative has the same structure as Lemma 1 (50). This guarantees fixed-time convergence for the states of altitude dynamics. ■

Remark 4: By utilizing the cascaded feature of the four-order strict-feedback altitude dynamics (6), the proposed transformational method (20)–(30) converts the output-feedback control problem for output-constrained system (6) into the one for an unconstrained system (30), which makes it possible to carry out output-feedback control design in the absence of recursive

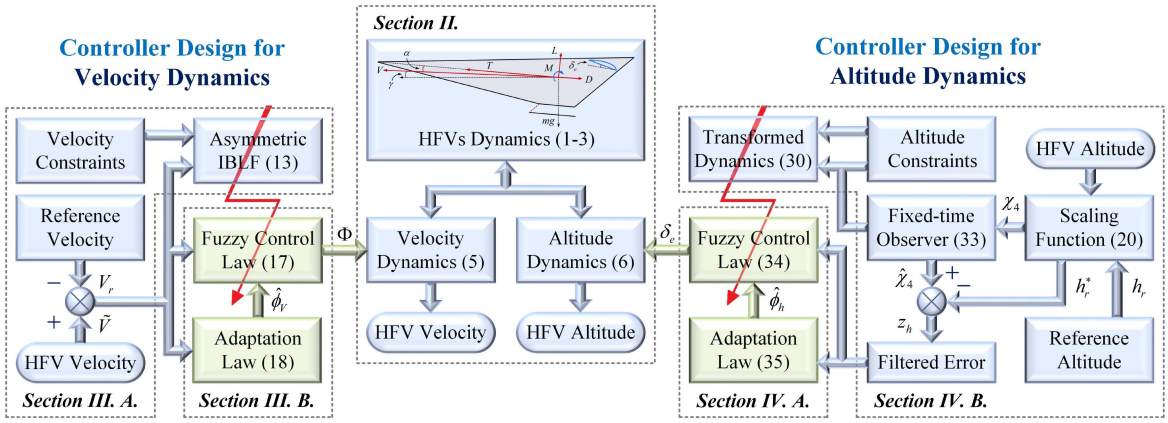

Fig. 1. Framework of the proposed control methodology.

design procedure. This is in contrast to the existing relevant works [8], [18], [23], [29], which are based on the backstepping-like framework; thus, it not only suffers from heavy computation burden in the sense of calculating massive differential equations as well as the derivatives of some intermediate control laws, but also requires four fuzzy logic approximators as well as four fixed-time observers for nonlinear approximation and compensation. On the contrary, our method (as sketched in Fig. 1) does not involve any recursive design steps and, thus, circumvents aforementioned issues relying on only one fuzzy logic approximator as well as one fixed-time differentiator.

Remark 5: In light of Theorems 1 and 2, for any initial conditions $V(0), h(0) \in \Omega_0$, the proposed output-feedback fixed-time trajectory tracking control methodology can guarantee that the output constraints (4) are never violated, i.e., $V(t), h(t) \in \Omega_0$ $\forall t \geq 0$. This further indicates that the compact set Ω_0 is an invariant set. As a result, our output-feedback control designs (17) and (34) not only ensure the boundedness of closed-loop signals but can also preserve the validity of fuzzy logic approximators.

V. Simulation Results

To illustrate the effectiveness and superiorities of the proposed backstepping-free output-feedback fixed-time trajectory tracking control scheme (PCS), several representative simulations are conducted in this section. The vehicle is assumed to climb a maneuver where the reference commands are set as an increment of 300 ft/s step signal in velocity dynamics and an increment of 3000 ft step signal in altitude dynamics. Additionally, to make the given reference commands more realizable, the trajectories of V_r and h_r and their derivatives are generated by filtering the reference commands via tracking differentiators [15]. Based on practical engineering characteristics, the limitations of the actuators are set as $\Phi \in [0.1, 1.2]$ and $\delta_e \in [-20^\circ, 20^\circ]$, and the output bounds are chosen as $V_{\max} = 11\,000$ ft/s, $V_{\min} = 7500$ ft/s, $h_{\max} = 135\,000$ ft, and $h_{\min} = 70\,000$ ft [7]. The uncertain aerodynamic coefficients in (3) are modeled as $C_i = C_i^*(1 + \Delta_i)$, where C_i^* represents the nominal coefficient and Δ_i represents the uncertain factor ranging from -30% to 30%. The external disturbances $\sin(\frac{\pi}{30}t)$ and $2\sin(\frac{\pi}{30}t)$ are added to velocity and altitude dynamics, respectively, when $t > 200$s.

The design parameters have various influences on the performance of the proposed scheme. In particular, setting bigger $k_{V,1}$, $k_{V,2}$, $k_{h,1}$, $k_{h,2}$, and p and smaller q, a_V, and a_h can lead to more accurate trajectory tracking maneuver with less settling time, but at the cost of increasing the amplitude of control signals. Thence, a tradeoff between the convergence performance and control action needs to be considered. In addition, choosing higher adaptation gains ρ_V and ρ_h can make the convergence rate faster, but result in more serious chattering phenomena. Besides, the small positive constants υ_V and υ_h are the σ-modification factors that can enhance the stability of $\widehat{\phi}_V$ and $\widehat{\phi}_h$ in the presence of approximation errors. On account of [39, Th. 3], $p_1 > 1$ and $0 < q_1 < 1$ should be selected close to 1. Subsequently, the estimation performance of the fixed-time differentiator can be improved by increasing τ_i and ι_i, $i \in \mathbb{N}_{1:4}$. Nevertheless, overly large τ_i and ι_i will increase the disturbance sensitivity of the differentiator. In engineering practice, τ_i and ι_i should be tuned appropriately in compromise between the antidisturbance performance and the estimation performance. As a result, the design parameters of control laws are chosen as $k_{V,1} = 2.5$, $k_{V,2} = 20$, $k_{h,1} = 15$, $k_{h,2} = 55$, $p = 5/3$, $q = 3/5$, $a_V = 0.75$, and $a_h = 1$, the design parameters of adaptation laws are selected as $c_V = 0.6$, $c_h = 1$, $\upsilon_V = 1$, and $\upsilon_h = 1.5$, and the design parameters of differentiator are set as $\tau_1 = \iota_1 = 2$, $\tau_2 = \iota_2 = 1.5$, $\tau_3 = \iota_3 = 0.5$, $\tau_4 = \iota_4 = 0.0625$, $p_1 = 1.1$, and $q_1 = 0.9$.

In the simulation studies, fuzzy IF–THEN rules for velocity dynamics are chosen as follows:

$$R^l: \text{If } V \text{ is } F_1^l \text{ and } V_r \text{ is } F_2^l \text{ and } \dot{V}_r \text{ is } F_3^l, \text{ then } y \text{ is } B^l$$

where $l \in \mathbb{N}_{1:5}$; the fuzzy sets are chosen as $F_j^1 = (\text{VS})$, $F_j^2 = (\text{SM})$, $F_j^3 = (\text{MI})$, $F_j^4 = (\text{BI})$, and $F_j^5 = (\text{VB})$, $j \in \mathbb{N}_{1:3}$, which are defined over the interval $[7500, 8400] \times [7600, 8300] \times [0, 12]$ for variables V, V_r, and $\dot{V}_r$. VS, SM, MI, BI, and VB indicate very small, small, middle, big, and very big, respectively. The corresponding fuzzy membership functions

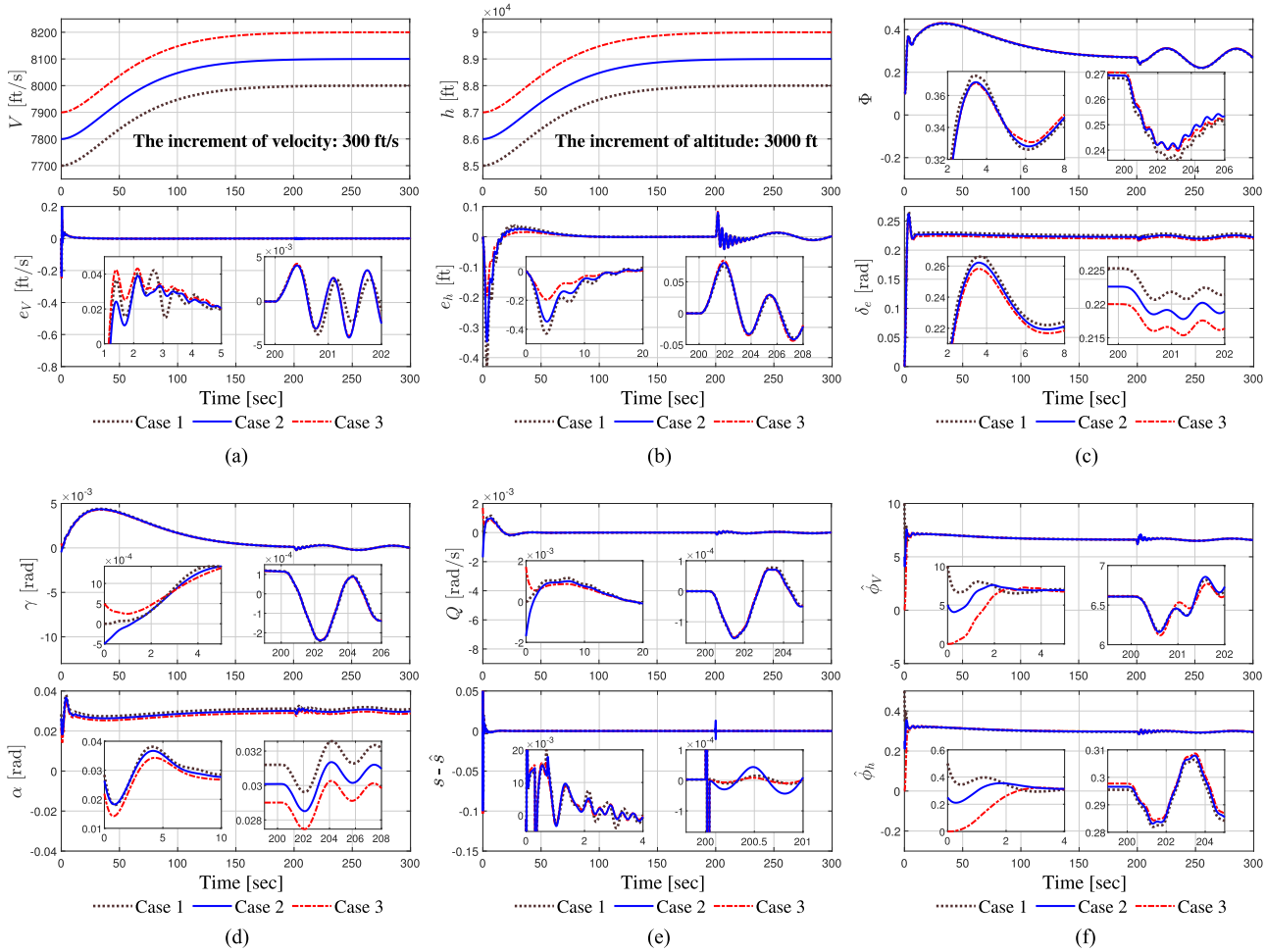

Fig. 2. Tracking performances, control inputs and flight states of the examined three cases. (a) Velocity tracking performances. (b) Altitude tracking performances. (c) Control inputs. (d) FPA and AOA. (e) Filtered error and pitch rate. (f) Weight values.

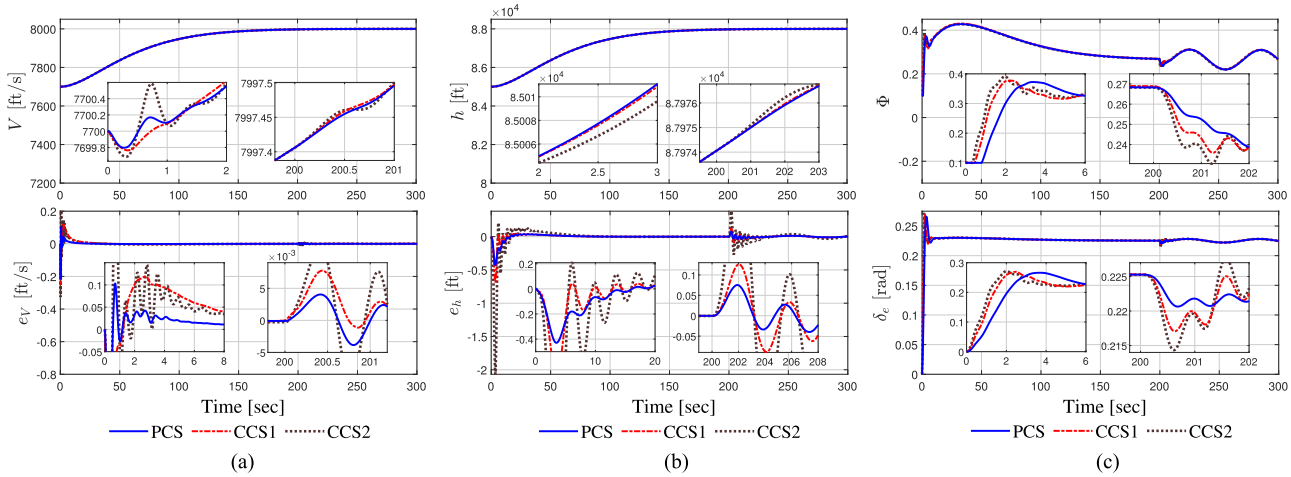

Fig. 3. Tracking performances and control inputs of the examined three control schemes. (a) Velocity tracking performances. (b) Altitude tracking performances. (c) Control inputs.

TABLE I
PERFORMANCE INDICES OF THE EXAMINED THREE CONTROL SCHEMES

Control Schemes	IAE		ITAE		RMSE		MACA	
	e_V	e_h	e_V	e_h	e_V	e_h	Φ	δ_e
PCS	0.4472	4.5879	16.6318	297.5327	0.0012	0.0460	0.3133	0.2260
CCS1	1.2498	4.8153	42.0769	346.9415	0.0077	0.0583	0.3139	0.2263
CCS2	1.2682	14.6109	52.0212	1061.1403	0.0193	0.1741	0.3148	0.2264

are chosen as follows:

$$\mu_{F_1^l}(V) = \exp\left[-\frac{(V-7275-225l)^2}{450}\right]$$
$$\mu_{F_2^l}(V_r) = \exp\left[-\frac{(V_r-7425-175l)^2}{350}\right]$$
$$\mu_{F_3^l}(\dot{V}_r) = \exp\left[-\frac{(\dot{V}_r+3-3l)^2}{6}\right], \quad l \in \mathbb{N}_{1:5}.$$

The fuzzy IF–THEN rules and fuzzy membership functions for altitude dynamics are similar to those of velocity dynamics. Most notably, with the aid of the proposed system transformational methodology, we solely employ one fuzzy logic approximator $F_h(\boldsymbol{x}_h)$ with $\boldsymbol{x}_h = [\boldsymbol{\chi}_4^\top, \boldsymbol{h}_r^\top]^\top$ for the four-order altitude dynamics (6), which is different from the existing backstepping-like works [5], [8], [18]. To be specific, in [5], there are four fuzzy logic approximators $F_h(\boldsymbol{x}_h)$, $F_\gamma(\boldsymbol{x}_\gamma)$, $F_\alpha(\boldsymbol{x}_\alpha)$, and $F_Q(\boldsymbol{x}_Q)$, with $\boldsymbol{x}_h = [h, h_r, h_r^{(1)}]^\top$, $\boldsymbol{x}_\gamma = [h, \gamma, h_r, h_r^{(1)}, h_r^{(2)}]^\top$, $\boldsymbol{x}_\alpha = [h, \gamma, \alpha, h_r, h_r^{(1)}, h_r^{(2)}, h_r^{(3)}]^\top$, and $\boldsymbol{x}_Q = [h, \gamma, \alpha, Q, h_r, h_r^{(1)}, h_r^{(2)}, h_r^{(3)}, h_r^{(4)}]^\top$. As a result, the total number of fuzzy rules associated with the partitioning of the HFV's state space is 20, the total numbers of fuzzy sets and the corresponding fuzzy membership functions that describe the HFV's state variables are both 120, and the total numbers of adjustable parameters such as centers and spreads of the fuzzy sets are both 120. On the contrary, PCS solely requires five fuzzy rules, 45 fuzzy sets, 45 fuzzy membership functions, 45 centers, and 45 spreads. This reveals that PCS exhibits a lower computation complexity than that of [5], [8], and [18].

A. Scenario 1

In order to show the practicability and robustness of PCS, the first scenario presents the simulation tests by taking the different initial values of rigid-body states and adaptation laws into account. The simulations in this scenario are divided into three cases.

1) *Case 1:* $V(0) = 7700$ ft/s, $h(0) = 85\,000$ ft, $\gamma(0) = 0$ rad, $\alpha(0) = 0.0284$ rad, $Q(0) = 0$ rad/s, $\widehat{\phi}_V(0) = 10$, and $\widehat{\phi}_h(0) = 0.5$.
2) *Case 2:* $V(0) = 7800$ ft/s, $h(0) = 86\,000$ ft, $\gamma(0) = -0.0005$ rad, $\alpha(0) = 0.0264$ rad, $Q(0) = -0.0017$ rad/s, $\widehat{\phi}_V(0) = 5$, and $\widehat{\phi}_h(0) = 0.25$.
3) *Case 3:* $V(0) = 7900$ ft/s, $h(0) = 87\,000$ ft, $\gamma(0) = 0.0005$ rad, $\alpha(0) = 0.0219$ rad, $Q(0) = 0.0017$ rad/s, $\widehat{\phi}_V(0) = 0$, and $\widehat{\phi}_h(0) = 0$.

Simulation results are depicted in Fig. 2(a)–(f). It is indicated from Fig. 2(a) and (b) that the velocity and altitude of HFV can track the reference trajectories in a rapid and precise manner when considering different initial conditions. The lower constraint on the velocity results in above Mach 5 curve, which confirms that the HFV was in the hypersonic regime throughout the flight. The altitude trajectory shows that only a small climbing maneuver is maintained by the controller, which indicates that the HFV was in cruise during the flight. Fig. 2(c) gives the time histories of the control inputs, including Φ and δ_e, implying that the actuators are free from chattering phenomena under three cases. Fig. 2(d) and (e) depicts the response curves of other rigid-body states of HFV. More concretely, the time histories of FPA, AOA, and pitch rate indicate that these attitude angles are all kept stable under three different initial values. Additionally, the estimation performances of the fixed-time differentiator are given in Fig. 2(e), which reveals that the filtered error can be estimated rapidly and effectively when considering aerodynamic coefficient uncertainties and external disturbances simultaneously. Subsequently, the approximations of weight values are depicted in Fig. 2(f), which shows that the performances of the weight values estimating in the three cases are both excellent.

B. Scenario 2

To illustrate the superiorities of proposed control scheme, the second scenario presents the comparative simulation tests among PCS and the existing approaches, i.e., the conventional backstepping-based control scheme (CCS1) [40] and the conventional PID control scheme (CCS2) [9]. Simulation results are depicted in Fig. 3(a)–(c). As shown in Fig. 3(a) and (b), PCS provides better transient and steady-state performance in comparison with CCS1 and CCS2 and ensures that V and h track the reference trajectories V_r and h_r with faster convergence speed. It can be observed that if the level of uncertainty lies in the interval $[-30\%, 30\%]$, the velocity and altitude curves obtained using asymmetric IBLF (13) and scaling function (20) are maintained within the imposed asymmetric constraints. It is clear from Fig. 3(c) that the control inputs obtained by PCS are smoother than that of CCS1 and CCS2, and the fuel equivalence ratios Φ get saturated only in initial 0–1 s. It can also be noted that PCS is effective in fast suppressing the sudden high-frequency transients in 200 s due to the introduction of fuzzy logic approximators. To further illustrate the tracking performance, the integral absolute error (IAE), integral time absolute error (ITAE), and root-mean-square error (RMSE) are introduced and defined as $\int_0^t |e(\tau)|\mathrm{d}\tau$, $\int_0^t t|e(\tau)|\mathrm{d}\tau$, and $(\frac{1}{t}\int_0^t e^2(\tau)\mathrm{d}\tau)^{\frac{1}{2}}$, respectively,

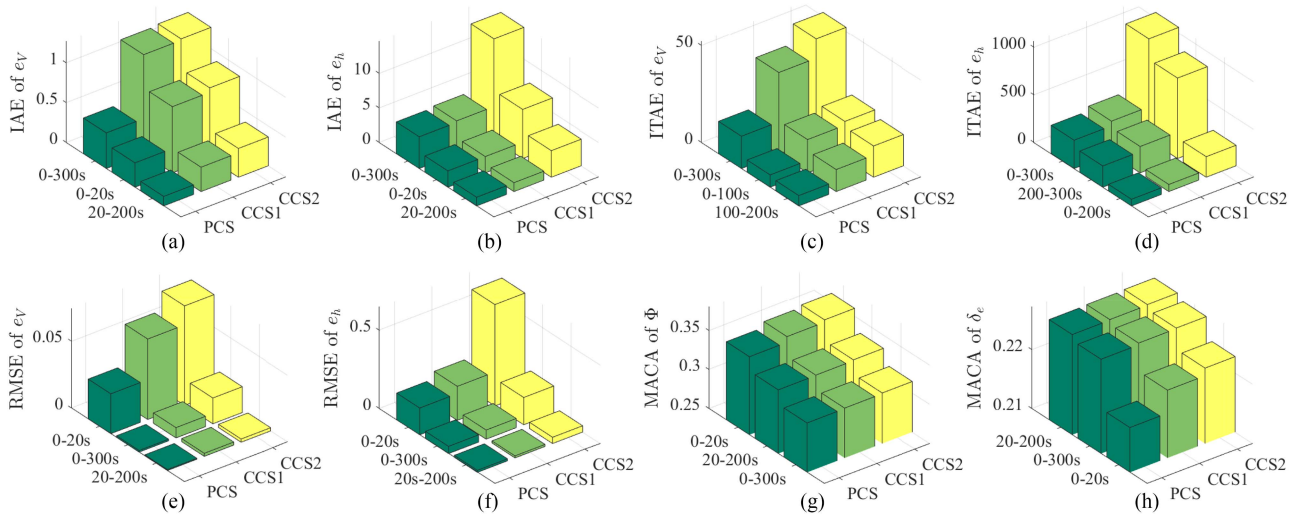

Fig. 4. (a)–(h) Performance indices of the examined three control schemes.

where t denotes the simulation time and e represents the tracking errors e_V and e_h. To assess the control energy quantitatively, the mean absolute control action (MACA) is introduced and defined as $\frac{1}{t}\int_0^t |u(\tau)|\mathrm{d}\tau$, where u represents the control inputs Φ and δ_e. The calculation results are summarized in Table I and Fig. 4. Fig. 4(a)–(f) shows that PCS exhibits less error energy than CCS1 and CCS2. Fig. 4(g) and (h) implies that the control effort of PCS is smaller than that of CCS1 and CCS2.

VI. Conclusion

This study investigates the output-feedback fixed-time trajectory tracking control problem for HFVs with asymmetric output constraints. The proposed control method is free from the conventional backstepping-like recursive framework, and the full-state information of HFVs is not required for control design. By utilizing the cascaded property of altitude dynamics as well as a novel scaling function, we convert the constrained system into an unconstrained one. Afterward, a fixed-time differentiator is used to ensure the tracking errors of velocity and altitude converge to the user-defined residual sets within fixed time. Future research will be concentrated on visual simulation and hardware in the loop simulation of the proposed control scheme, and the flatness-based adaptive fuzzy control design for HFV swarm systems [41]–[44].

Appendix
Proof of Theorem 1

We begin the proof with the introduction of the compact set $\Omega_V \triangleq \{\boldsymbol{\eta}_V | L_V \leq \varrho_V\}$ about the vector $\boldsymbol{\eta}_V = [\widetilde{V}, \widetilde{\phi}_V]^\top$. Then, by combining (17) and (18) with (19), the time derivative of L_V is

$$\begin{aligned}\dot{L}_V \leq & -k_{V,1}\beta^{\frac{p+1}{2}}\widetilde{V}^{p+1} - k_{V,2}\beta^{\frac{q+1}{2}}\widetilde{V}^{q+1} \\ & + \upsilon_V \widetilde{\phi}_V \widehat{\phi}_V + \frac{a_V^2}{2} + \frac{\varepsilon_V^{*2}}{2}. \end{aligned} \tag{37}$$

Invoking Young's inequality [40], $\widetilde{\phi}_V\widehat{\phi}_V$ in (37) satisfies $\widetilde{\phi}_V\widehat{\phi}_V \leq \widetilde{\phi}_V(\phi_V - \widetilde{\phi}_V) \leq \frac{c_V}{2}\phi_V^2 - \frac{1}{\rho_V}\widetilde{\phi}_V^2$; then, one has

$$\begin{aligned}\dot{L}_V \leq & -k_{V,1}\beta^{\frac{p+1}{2}}\widetilde{V}^{p+1} - k_{V,2}\beta^{\frac{q+1}{2}}\widetilde{V}^{q+1} - \upsilon_V\left(\frac{\widetilde{\phi}_V^2}{2\rho_V}\right)^{\frac{p+1}{2}} \\ & - \upsilon_V\left(\frac{\widetilde{\phi}_V^2}{2\rho_V}\right)^{\frac{q+1}{2}} + \upsilon_V\left(\frac{\widetilde{\phi}_V^2}{2\rho_V}\right)^{\frac{p+1}{2}} + \upsilon_V\left(\frac{\widetilde{\phi}_V^2}{2\rho_V}\right)^{\frac{q+1}{2}} \\ & - \frac{\upsilon_V}{\rho_V}\widetilde{\phi}_V^2 + \frac{c_V\upsilon_V}{2}\phi_V^2 + \frac{a_V^2}{2} + \frac{\varepsilon_V^{*2}}{2}. \end{aligned} \tag{38}$$

According to Lemma 4, it holds that $(\frac{\widetilde{\phi}_V^2}{2\rho_V})^{\frac{q+1}{2}} \leq \frac{\widetilde{\phi}_V^2}{2\rho_V} + \frac{1-q}{2}(\frac{2}{1+q})^{-\frac{1+q}{1-q}}$. Substituting this inequality into (38) gives

$$\begin{aligned}\dot{L}_V \leq & -k_{V,1}\beta^{\frac{p+1}{2}}\widetilde{V}^{p+1} - k_{V,2}\beta^{\frac{q+1}{2}}\widetilde{V}^{q+1} - \upsilon_V\left(\frac{\widetilde{\phi}_V^2}{2\rho_V}\right)^{\frac{p+1}{2}} \\ & - \upsilon_V\left(\frac{\widetilde{\phi}_V^2}{2\rho_V}\right)^{\frac{q+1}{2}} + \upsilon_V\left(\frac{\widetilde{\phi}_V^2}{2\rho_V}\right)^{\frac{p+1}{2}} - \frac{\upsilon_V}{2\rho_V}\widetilde{\phi}_V^2 + \mu_{V,0} \end{aligned} \tag{39}$$

where $\mu_{V,0} = \frac{(1-q)\upsilon_V}{2}(\frac{2}{1+q})^{-\frac{1+q}{1-q}} + \frac{c_V\upsilon_V\phi_V^2}{2} + \frac{a_V^2}{2} + \frac{\varepsilon_V^{*2}}{2}$.

With the aid of Lemma 5, (39) can be rewritten as

$$\begin{aligned}\dot{L}_V \leq & -\kappa_{V,1}L_V^{\frac{p+1}{2}} - \kappa_{V,2}L_V^{\frac{q+1}{2}} + \upsilon_V\left(\frac{\widetilde{\phi}_V^2}{2\rho_V}\right)^{\frac{p+1}{2}} \\ & - \frac{\upsilon_V}{2\rho_V}\widetilde{\phi}_V^2 + \mu_{V,0} \end{aligned} \tag{40}$$

on the compact set $\Omega_V \times \Omega_r \times \Omega_0$, where $\kappa_{V,1} = \min\{k_{V,1}, \upsilon_V\}$ and $\kappa_{V,2} = \min\{k_{V,2}, \upsilon_V\}$.

Assume that there exists an unknown positive constant Θ_V such that $|\widetilde{\phi}_V| \leq \Theta_V$. The following two cases need to be considered: 1) if $\Theta_V < \sqrt{2\rho_V}$, one has $\upsilon_V(\frac{\widetilde{\phi}_V^2}{2\rho_V})^{\frac{p+1}{2}} - \frac{\upsilon_V}{2\rho_V}\widetilde{\phi}_V^2 < 0$

and 2) if $\Theta_V \geq \sqrt{2\rho_V}$, one has $\upsilon_V(\frac{\widetilde{\phi}_V^2}{2\rho_V})^{\frac{p+1}{2}} - \frac{\upsilon_V}{2\rho_V}\widetilde{\phi}_V^2 \leq \frac{\upsilon_V}{2\rho_V}\Theta_V^2 + \upsilon_V(\frac{\Theta_V^2}{2\rho_V})^{\frac{p+1}{2}}$. Summarizing above two cases gives

$$\upsilon_V\left(\frac{\widetilde{\phi}_V^2}{2\rho_V}\right)^{\frac{p+1}{2}} - \frac{\upsilon_V}{2\rho_V}\widetilde{\phi}_V^2 + \mu_{V,0} \leq \mu_{V,1} \tag{41}$$

where

$$\mu_{V,1} = \begin{cases} \mu_{V,0}, & \text{if } \Theta_V < \sqrt{2\rho_V} \\ \mu_{V,0} + \upsilon_V\left(\frac{\Theta_V^2}{2\rho_V}\right)^{\frac{p+1}{2}} + \frac{\upsilon_V}{2\rho_V}\Theta_V^2, & \text{otherwise.} \end{cases}$$

Substituting (41) into (40), it can be inferred that

$$\dot{L}_V \leq -\kappa_{V,1}L_V^{\frac{p+1}{2}} - \kappa_{V,2}L_V^{\frac{q+1}{2}} + \mu_{V,1} \tag{42}$$

holds on the compact set $\Omega_V \times \Omega_r \times \Omega_0$.

Note that $\frac{\mu_{V,1}}{\kappa_{V,1}}$ can be made arbitrarily small by decreasing a_V and c_V, meanwhile increasing $k_{V,2}$ and υ_V. Thence, we can obtain $\frac{\mu_{V,1}}{\kappa_{V,1}} \leq \varrho_V^{\frac{p+1}{2}}$ by choosing appropriate design parameters. Since $\frac{\mu_{V,1}}{\kappa_{V,1}} \leq \varrho_V^{\frac{p+1}{2}}$, one has $\dot{L}_V \leq -\kappa_{V,2}L_V^{\frac{q+1}{2}} \leq 0$ on $L_V = \varrho_V$ according to (42). As such, $L_V \leq \varrho_V$ holds $\forall t \geq 0$. The boundedness of L_V implies the boundedness of $L_{\widetilde{V}}$, which indicates that the asymmetric output constraints (4) are never violated. As a result, it is concluded that $\Omega_V \times \Omega_r \times \Omega_0$ is an invariant set, and thus, all the signals in velocity dynamics (5) are SGUUB.

Noting that when $L_V^{\frac{p+1}{2}} \geq \frac{\mu_{V,1}}{\varpi_V\kappa_{V,1}}$ for $0 < \varpi_V < 1$, one has $\mu_{V,1} \leq \varpi_V\kappa_{V,1}L_V^{\frac{p+1}{2}}$. Thus, following (42), we obtain

$$\dot{L}_V \leq -(1-\varpi_V)\kappa_{V,1}L_V^{\frac{p+1}{2}} - \kappa_{V,2}L_V^{\frac{q+1}{2}}. \tag{43}$$

Employing (43) and Lemma 1, L_V will converge to the set $\Omega_{L_V} = \left\{L_V \mid L_V < (\frac{\mu_{V,1}}{\varpi_V\kappa_{V,1}})^{\frac{2}{p+1}}\right\}$ in fixed time with the guaranteed convergence time estimated as follows:

$$T_V \leq T_{V,\max} \triangleq \frac{2}{\kappa_{V,1}(1-\varpi_V)(p-1)} + \frac{2}{\kappa_{V,2}(1-q)}.$$

Recalling the construction of $L_{\widetilde{V}}$ in (13), it is straightforward to deduce that $\widetilde{V}$ will converge to the set $\Omega_{\widetilde{V}} = \left\{\widetilde{V} \;\middle|\; |\widetilde{V}| < \sqrt{2(\frac{\mu_{V,1}}{\varpi_V\kappa_{V,1}})^{\frac{2}{p+1}}}\right\}$ in fixed time with the guaranteed convergence time estimated as T_V. ■

Proof of Theorem 2

Initially, consider the compact set $\Omega_h \triangleq \{\boldsymbol{\eta}_h | L_h \leq \varrho_h\}$ about the vector $\boldsymbol{\eta}_h = [\widetilde{h}, \widetilde{\phi}_h]^\top$. Then, differentiating (36) with respect to time gives

$$\begin{aligned}\dot{L}_h = {} & g_\chi(\boldsymbol{\chi}_4)\left\{-k_{h,1}s\widehat{s}^p - \frac{s\widehat{s}\widehat{\phi}_h}{2a_h^2}\boldsymbol{\varphi}_h^\top(\widehat{\boldsymbol{x}}_h)\boldsymbol{\varphi}_h(\widehat{\boldsymbol{x}}_h) - k_{h,2}s\widehat{s}^q\right\} \\ & + \frac{s^2\phi_h}{2a_h^2}\boldsymbol{\varphi}_h^\top(\boldsymbol{x}_h)\boldsymbol{\varphi}_h(\boldsymbol{x}_h) - \frac{\widehat{s}^2\widetilde{\phi}_h}{2a_h^2}\boldsymbol{\varphi}_h^\top(\widehat{\boldsymbol{x}}_h)\boldsymbol{\varphi}_h(\widehat{\boldsymbol{x}}_h) \\ & + \frac{a_h^2}{2} + \frac{\varepsilon_h^{*2}}{2} + \upsilon_h\widetilde{\phi}_h\widehat{\phi}_h. \end{aligned} \tag{44}$$

By defining $\widetilde{s} = s - \widehat{s}$, (44) can be rewritten as

$$\begin{aligned}\dot{L}_h = {} & -g_\chi(\boldsymbol{\chi}_4)k_{h,1}s^{p+1} - g_\chi(\boldsymbol{\chi}_4)k_{h,2}s^{q+1} \\ & + \frac{a_h^2}{2} + \frac{\varepsilon_h^{*2}}{2} + \upsilon_h\widetilde{\phi}_h\widehat{\phi}_h + \Xi_h \end{aligned} \tag{45}$$

with $\Xi_h = \frac{s^2\phi_h}{2a_h^2}\boldsymbol{\varphi}_h^\top(\boldsymbol{x}_h)\boldsymbol{\varphi}_h(\boldsymbol{x}_h) - \frac{\widehat{s}^2\widetilde{\phi}_h}{2a_h^2}\boldsymbol{\varphi}_h^\top(\widehat{\boldsymbol{x}}_h)\boldsymbol{\varphi}_h(\widehat{\boldsymbol{x}}_h) + g_\chi(\boldsymbol{\chi}_4) \times \left\{-k_{h,1}s(\widehat{s}^p - s^p) - k_{h,2}s(\widehat{s}^q - s^q) - \frac{s\widehat{s}\widehat{\phi}_h}{2a_h^2}\boldsymbol{\varphi}_h^\top(\widehat{\boldsymbol{x}}_h)\boldsymbol{\varphi}_h(\widehat{\boldsymbol{x}}_h)\right\}$.

Based on Lemma 7, the rest of the proof will be divided into the following two steps.

Step 1: First, it will be shown that the system states do not escape to infinity during $t \in [0, T_1]$. Invoking the boundedness of $\widetilde{\boldsymbol{\chi}}_4$, we can further obtain that

$$\begin{aligned} |s - \widehat{s}| &\leq \left|\left|[\boldsymbol{\Lambda} \;\; 1]\right|\right| \left|\left|\widetilde{\boldsymbol{\chi}}_4\right|\right| \triangleq o_s \\ |s^p - \widehat{s}^p| &\leq |ps_0^{p-1}|\,|s - \widehat{s}| \triangleq o_{s^p} \\ |s^q - \widehat{s}^q| &\leq |s - \widehat{s}| + 2 \triangleq o_{s^q} \end{aligned} \tag{46}$$

where the mean value theory [45] is used with $s_0 = \rho_0(s - \widehat{s}) + \widehat{s}$ and $\rho_0 \in (0,1)$. Recalling the definition of FLS, it holds that $0 < \boldsymbol{\varphi}^\top(\cdot)\boldsymbol{\varphi}(\cdot) < 1$ and thus $|\boldsymbol{\varphi}_h^\top(\boldsymbol{x}_h)\boldsymbol{\varphi}_h(\boldsymbol{x}_h) - \boldsymbol{\varphi}_h^\top(\widehat{\boldsymbol{x}}_h)\boldsymbol{\varphi}_h(\widehat{\boldsymbol{x}}_h)| < 1$. Incorporating (46) into (45) gives

$$\dot{L}_h \leq \frac{1}{2}\Xi_s s^2 + \frac{1}{2}\Xi_{\phi_h}\widetilde{\phi}_h^2 + \omega_0 \tag{47}$$

where

$$\begin{aligned} \omega_0 = {} & \frac{g_{\chi,\max}o_s o_{W_h}}{4g_{\chi,\min}a_h^2} + \frac{c_h\upsilon_h o_{W_h}^2}{2} + \frac{o_{s^2}}{4a_h^2} + \frac{\varepsilon_h^{*2}}{2} \\ & + \frac{g_{\chi,\max}k_{h,1}o_{s^p}}{2} + \frac{g_{\chi,\max}k_{h,2}o_{s^q}}{2} + \frac{a_h^2}{2} \\ \Xi_s = {} & \frac{g_{\chi,\max}o_s o_{W_h}}{2g_{\chi,\min}a_h^2} + \frac{g_{\chi,\max}o_s}{2g_{\chi,\min}a_h^2} + \frac{2o_{W_h}}{a_h^2} \\ & + g_{\chi,\max}k_{h,1}o_{s^p} + g_{\chi,\max}k_{h,2}o_{s^q} \\ \Xi_{\phi_h} = {} & \frac{g_{\chi,\max}o_s}{2g_{\chi,\min}a_h^2} + \frac{o_{s^2}}{2a_h^2}. \end{aligned}$$

Thus, (47) can be rewritten as

$$\dot{L}_h \leq \omega_h L_h + \omega_0 \tag{48}$$

where $\omega_h = \max\{\Xi_s, \rho_h\Xi_{\phi_h}\}$. Solving inequality (48) obtains $L_h(t) \leq (L_h(0) + \frac{\omega_0}{\omega_h})\exp(\omega_h T_1)$ for all $t \in [0, T_1]$; thus, the closed-loop system states will not escape to infinity during $t \in [0, T_1]$.

Step 2: Then, the fixed-time convergence of the closed-loop system states will be proven in this step. From (45), one has

$$\begin{aligned}\dot{L}_h \leq {} & -k_{h,1}g_{\chi,\min}s^{p+1} - k_{h,2}g_{\chi,\min}s^{q+1} \\ & + \upsilon_h\widetilde{\phi}_h\widehat{\phi}_h + \frac{a_h^2}{2} + \frac{\varepsilon_h^{*2}}{2}. \end{aligned} \tag{49}$$

The rest of the proof does not much differ from that of the velocity dynamics and, thus, is omitted here for brevity. Similarly and iteratively, it is possible to arrive

$$\dot{L}_h \leq -\kappa_{h,1}L_h^{\frac{p+1}{2}} - \kappa_{h,2}L_h^{\frac{q+1}{2}} + \mu_{h,1} \tag{50}$$

in which constants $\kappa_{h,1} = \min\{k_{h,1}g_{\chi,\min}, \frac{\upsilon_h}{g_{\chi,\min}}\}$, $\kappa_{h,2} = \min\{k_{h,2}g_{\chi,\min}, \frac{\upsilon_h}{g_{\chi,\min}}\}$, and

$$\mu_{h,1} = \begin{cases} \mu_{h,0}, & \text{if } \Theta_h < \sqrt{2\rho_h} \\ \mu_{h,0} + \frac{\upsilon_h}{g_{\chi,\min}}\left(\frac{\Theta_h^2}{2\rho_h}\right)^{\frac{p+1}{2}} + \frac{\upsilon_h}{2\rho_h g_{\chi,\min}}\Theta_h^2, & \text{otherwise} \end{cases}$$

with $\mu_{h,0} = \frac{(1-q)\upsilon_h}{2g_{\chi,\min}}(\frac{2}{1+q})^{-\frac{1+q}{1-q}} + \frac{c_h\upsilon_h\phi_h^2}{2g_{\chi,\min}} + \frac{a_h^2}{2} + \frac{\varepsilon_h^{*2}}{2}$ and unknown positive constant Θ_h satisfying $|\widetilde{\phi}_h| \le \Theta_h$.

Note that $\frac{\mu_{h,1}}{\kappa_{h,1}}$ can be made arbitrarily small by decreasing a_h and c_h, meanwhile increasing $k_{h,2}$ and υ_h. Thence, we can obtain $\frac{\mu_{h,1}}{\kappa_{h,1}} \le \varrho_h^{\frac{p+1}{2}}$ by choosing appropriate design parameters. Since $\frac{\mu_{h,1}}{\kappa_{h,1}} \le \varrho_h^{\frac{p+1}{2}}$, one has $\dot{L}_h \le -\kappa_{h,2}L_h^{\frac{q+1}{2}} \le 0$ on $L_h = \varrho_h$ according to (50). As such, $L_h \le \varrho_h$ holds $\forall t \ge 0$. The boundedness of L_h implies the boundedness of $L_{\widetilde{h}}$, which indicates that the asymmetric output constraints (4) are never violated. As a result, it is concluded that $\Omega_h \times \Omega_r \times \Omega_0$ is an invariant set, and thus, all the signals in velocity dynamics (5) are SGUUB.

Similarly, for $0 < \varpi_h < 1$, L_h will converge to the set $\Omega_{L_h} = \left\{L_h \;\middle|\; L_h < (\frac{\mu_{h,1}}{\varpi_h\kappa_{h,1}})^{\frac{2}{p+1}}\right\}$ in fixed time with the guaranteed convergence time estimated as follows:

$$T_h \le T_{h,\max} \triangleq \frac{2}{\kappa_{h,1}(1-\varpi_h)(p-1)} + \frac{2}{\kappa_{h,2}(1-q)}.$$

Recalling the construction of L_h in (36), it is straightforward to deduce that s will converge to the set $\Omega_s = \left\{s \;\middle|\; |s| < \sqrt{2(\frac{\mu_{h,1}}{\varpi_h\kappa_{h,1}})^{\frac{2}{p+1}}}\right\}$ in fixed time with the guaranteed convergence time estimated as T_h. ■

REFERENCES

[1] Q. Shen, B. Jiang, and V. Cocquempot, "Fault-tolerant control for T-S fuzzy systems with application to near-space hypersonic vehicle with actuator faults," *IEEE Trans. Fuzzy Syst.*, vol. 20, no. 4, pp. 652–665, Aug. 2012.

[2] H. Wu, Z. Liu, and L. Guo, "Robust L_∞-gain fuzzy disturbance observer-based control design with adaptive bounding for a hypersonic vehicle," *IEEE Trans. Fuzzy Syst.*, vol. 22, no. 6, pp. 1401–1412, Dec. 2014.

[3] R. Zuo, Y. Li, M. Lv, and Z. Liu, "Realization of trajectory precise tracking for hypersonic flight vehicles with prescribed performances," *Aerosp. Sci. Technol.*, vol. 111, Apr. 2021, Art. no. 106554.

[4] L. Fiorentini and A. Serrani, "Adaptive restricted trajectory tracking for a non-minimum phase hypersonic vehicle model," *Automatica*, vol. 48, no. 7, pp. 1248–1261, Jul. 2012.

[5] M. Lv, Y. Li, W. Pan, and S. Baldi, "Finite-time fuzzy adaptive constrained tracking control for hypersonic flight vehicles with singularity-free switching," *IEEE/ASME Trans. Mechatronics*, early access, doi: 10.1109/TMECH.2021.3090509.

[6] M. A. Bolender and D. B. Doman, "Nonlinear longitudinal dynamical model of an air-breathing hypersonic vehicle," *J. Spacecraft Rockets*, vol. 44, no. 2, pp. 374–387, Feb. 2007.

[7] L. Fiorentini, A. Serrani, M. A. Bolender, and D. B. Doman, "Nonlinear robust adaptive control of flexible air-breathing hypersonic vehicles," *J. Guid., Control, Dyn.*, vol. 32, no. 2, pp. 402–417, Mar. 2009.

[8] K. P. Tee and S. S. Ge, "Barrier Lyapunov functions for the control of output-constrained nonlinear systems," *Automatica*, vol. 45, no. 4, pp. 918–927, Apr. 2009.

[9] B. Xu, Z. Shi, F. Sun, and W. He, "Barrier Lyapunov function based learning control of hypersonic flight vehicle with AOA constraint and actuator faults," *IEEE Trans. Cybern.*, vol. 49, no. 3, pp. 1047–1057, Mar. 2019.

[10] Y. Li, Y. Liu, and S. Tong, "Observer-based neuro-adaptive optimized control for a class of strict-feedback nonlinear systems with state constraints," *IEEE Trans. Neural Netw. Learn. Syst.*, early access, doi: 10.1109/TNNLS.2021.3051030.

[11] S. S. Ge, C. C. Hang, and T. Zhang, "A direct adaptive controller for dynamic systems with a class of nonlinear parameterizations," *Automatica*, vol. 35, no. 4, pp. 741–747, Apr. 1999.

[12] K. P. Tee and S. S. Ge, "Control of state-constrained nonlinear systems using integral barrier Lyapunov functionals," in *Proc. IEEE Conf. Decis. Control*, 2012, pp. 3239–3244.

[13] D. Swaroop, J. K. Hedrick, P. P. Yip, and J. C. Gerdes, "Dynamic surface control for a class of nonlinear systems," *IEEE Trans. Autom. Control*, vol. 45, no. 10, pp. 1893–1899, Oct. 2000.

[14] J. H. Park, S. H. Kim, and C. J. Moon, "Adaptive neural control for strict-feedback nonlinear systems without backstepping," *IEEE Trans. Neural Netw. Learn. Syst.*, vol. 20, no. 7, pp. 1204–1209, Jul. 2009.

[15] X. Bu, Y. Xiao, and H. Lei, "An adaptive critic design-based fuzzy neural controller for hypersonic vehicles: Predefined behavioral nonaffine control," *IEEE/ASME Trans. Mechatronics*, vol. 24, no. 4, pp. 1871–1881, Aug. 2019.

[16] X. Bu, "Envelope-constraint-based tracking control of air-breathing hypersonic vehicles," *Aerosp. Sci. Technol.*, vol. 95, Dec. 2019, Art. no. 105429.

[17] W. Meng, Q. Yang, S. Jagannathan, and Y. Sun, "Adaptive neural control of high-order uncertain nonaffine systems: A transformation to affine systems approach," *Automatica*, vol. 50, no. 5, pp. 1473–1480, May 2014.

[18] Z. Liu, X. Tan, R. Yuan, G. Fan, and J. Yi, "Immersion and invariance-based output feedback control of air-breathing hypersonic vehicles," *IEEE Trans. Autom. Sci. Eng.*, vol. 13, no. 1, pp. 394–402, Jan. 2016.

[19] Y. Li, S. Tong, and T. Li, "Hybrid fuzzy adaptive output feedback control design for uncertain MIMO nonlinear systems with time-varying delays and input saturation," *IEEE Trans. Fuzzy Syst.*, vol. 24, no. 4, pp. 841–853, Aug. 2016.

[20] H. Li, Y. Pan, P. Shi, and Y. Shi, "Switched fuzzy output feedback control and its application to a mass-spring-damping system," *IEEE Trans. Fuzzy Syst.*, vol. 24, no. 6, pp. 1259–1269, Dec. 2016.

[21] X. Zhao, X. Wang, G. Zong, and H. Li, "Fuzzy-approximation-based adaptive output-feedback control for uncertain nonsmooth nonlinear systems," *IEEE Trans. Fuzzy Syst.*, vol. 26, no. 6, pp. 3847–3859, Dec. 2018.

[22] Y. Li, T. Yang, and S. Tong, "Adaptive neural networks finite-time optimal control for a class of nonlinear systems," *IEEE Trans. Neural Netw. Learn. Syst.*, vol. 31, no. 11, pp. 4451–4460, Nov. 2020.

[23] J. Sun, J. Yi, Z. Pu, and Z. Liu, "Adaptive fuzzy nonsmooth backstepping output-feedback control for hypersonic vehicles with finite-time convergence," *IEEE Trans. Fuzzy Syst.*, vol. 28, no. 10, pp. 2320–2334, Oct. 2020.

[24] Y. Li, K. Li, and S. Tong, "Adaptive neural network finite-time control for multi-input and multi-output nonlinear systems with the powers of odd rational numbers," *IEEE Trans. Neural Netw. Learn. Syst.*, vol. 31, no. 7, pp. 2532–2543, Jul. 2020.

[25] X. Yu, P. Li, and Y. Zhang, "The design of fixed-time observer and finite-time fault-tolerant control for hypersonic gliding vehicles," *IEEE Trans. Ind. Electron.*, vol. 65, no. 5, pp. 4135–4144, May 2018.

[26] A. Polyakov, "Nonlinear feedback design for fixed-time stabilization of linear control systems," *IEEE Trans. Autom. Control*, vol. 57, no. 8, pp. 2106–2110, Aug. 2012.

[27] B. Tian, Z. Zuo, X. Yan, and H. Wang, "A fixed-time output feedback control scheme for double integrator systems," *Automatica*, vol. 80, pp. 17–24, Jun. 2017.

[28] R. Zuo, Y. Li, M. Lv, Z. Liu, and Z. Dong, "Design of singularity-free fixed-time fault-tolerant control for HFVs with guaranteed asymmetric time-varying flight state constraints," *Aerosp. Sci. Technol.*, vol. 120, Jan. 2022, Art. no. 107270.

[29] J. Sun, Z. Pu, J. Yi, and Z. Liu, "Fixed-time control with uncertainty and measurement noise suppression for hypersonic vehicles via augmented sliding mode observers," *IEEE Trans. Ind. Inform.*, vol. 16, no. 2, pp. 1192–1203, Feb. 2020.

[30] J. T. Parker, A. Serrani, S. Yurkovich, M. A. Bolender, and D. B. Doman, "Control-oriented modeling of an air-breathing hypersonic vehicle," *J. Guid., Control, Dyn.*, vol. 30, no. 3, pp. 856–869, May 2007.

[31] M. Hazewinkel, *Encyclopaedia of Mathematics*. Norwell, MA, USA: Kluwer, 2002.

[32] M. Lv, W. Yu, J. Cao, and S. Baldi, "Consensus in high-power multi-agent systems with mixed unknown control directions via hybrid Nussbaum-based control," *IEEE Trans. Cybern.*, early access, doi: 10.1109/TCYB.2020.3028171.

[33] S. Sui, C. L. P. Chen, and S. Tong, "Neural network filtering control design for nontriangular structure switched nonlinear systems in finite time," *IEEE Trans. Neural Netw. Learn. Syst.*, vol. 30, no. 7, pp. 2153–2162, Jul. 2019.

[34] M. Lv, B. De J. S. Cao, and S. Baldi, "Adaptive prescribed performance asymptotic tracking for high-order odd-rational-power nonlinear systems," *IEEE Trans. Autom. Control*, early access, doi: 10.1109/TAC.2022.3147271.

[35] M. Lv, W. Yu, and S. Baldi, "The set-invariance paradigm in fuzzy adaptive DSC design of large-scale nonlinear input-constrained systems," *IEEE Trans. Syst., Man, Cybern., Syst.*, vol. 51, no. 2, pp. 1035–1045, Feb. 2021.

[36] L. Wang, *Adaptive Fuzzy Systems and Control: Design and Stability Analysis*. Englewood Cliffs, NJ, USA: Prentice-Hall, 1994.

[37] S. Sui, C. L. P. Chen, and S. Tong, "Fuzzy adaptive finite-time control design for nontriangular stochastic nonlinear systems," *IEEE Trans. Fuzzy Syst.*, vol. 27, no. 1, pp. 172–184, Jan. 2019.

[38] V. Kostrykin and A. Oleynik, "An intermediate value theorem for monotone operators in ordered Banach spaces," *Fixed Point Theory Appl.*, vol. 211, no. 1, pp. 1–4, Nov. 2012.

[39] M. V. Basin, P. Yu, and Y. B. Shtessel, "Hypersonic missile adaptive sliding mode control using finite- and fixed-time observers," *IEEE Trans. Ind. Electron.*, vol. 65, no. 1, pp. 930–941, Jan. 2018.

[40] R. Zuo, X. Dong, Y. Liu, Z. Liu, and W. Zhang, "Adaptive neural control for MIMO pure-feedback nonlinear systems with periodic disturbances," *IEEE Trans. Neural Netw. Learn. Syst.*, vol. 30, no. 6, pp. 1756–1767, Jun. 2019.

[41] M. Lv, W. Yu, J. Cao, and S. Baldi, "A separation-based methodology to consensus tracking of switched high-order nonlinear multi-agent systems," *IEEE Trans. Neural Netw. Learn. Syst.*, early access, doi: 10.1109/TNNLS.2021.3070824.

[42] G. Rigatos, "Flatness-based adaptive fuzzy control for nonlinear dynamical systems," in *Proc. IEEE/ASME Int. Conf. Adv. Intell. Mechatronics*, 2011, pp. 1016–1021.

[43] G. Rigatos, P. Siano, and S. Ademi, "Flatness-based adaptive fuzzy control of brushless doubly-fed reluctance machines," in *Proc. IEEE Int. Symp. Ind. Electron.*, 2017, pp. 1913–1920.

[44] M. Lv, B. De Schutter, C. Shi, and S. Baldi, "Logic-based distributed switching control for agents in power-chained form with multiple unknown control directions," *Automatica*, vol. 137, Mar. 2022, Art. no. 110143.

[45] H. K. Khalil, *Nonlinear Systems*. 3rd ed. Upper Saddle River, NJ, USA: Prentice-Hall, 2002.